UNIVERSIDADE DE LISBOA
FACULDADE DE CIÊNCIAS
DEPARTAMENTO DE ENGENHARIA GEOGRÁFICA, GEOFÍSICA E ENERGIA

Single Channel Model for Flow and Heat Transfer in High Temperature Solar Volumetric Air Receiver

Ana Luísa Oliveira Tostão

Dissertação

Mestrado Integrado em Engenharia da Energia e do Ambiente

2015

UNIVERSIDADE DE LISBOA
FACULDADE DE CIÊNCIAS
DEPARTAMENTO DE ENGENHARIA GEOGRÁFICA,
GEOFÍSICA E ENERGIA

Single Channel Model for Flow and Heat Transfer in High Temperature Solar Volumetric Air Receiver

Ana Luísa Oliveira Tostão

Dissertação

Mestrado Integrado em Engenharia da Energia e do Ambiente

Trabalho realizado sob a supervisão de

Cristiano Teixeira Boura (SIJ)

Maria João Carvalho (FCUL)

2015

Acknowledgements

I would like to thank to my co-supervisor Mr. Cristiano Boura for giving me the chance to do this thesis and my supervisor Professor Maria João Carvalho, to them my thank you for the support, contribution and guidance in this work. Solar Institute Jülich for allowing me to develop this work using their resources.

I would like to thank also to Mr. Behzad Alebouy for his help, support, cooperation and encouragement which was a crucial help at a certain time for the development of the work.

Finally I want to thank to my family who made a big effort to help me and support me not only in this time of the development of this work but also along this period of studies, to my boyfriend who supported me and encouraged me in the most difficult periods of this work and to all the people that direct or indirectly helped and supported me.

Abstract

In a first approach, this thesis presents a state of the art about the main general technology, Concentrating Solar Power Plants and posteriorly a description about the air solar receiver technology focusing the main features, parameters and developments.

This thesis presents also a model of a high temperature air solar receiver modeled in simulation software, COMSOL Multiphysics ® using silicon carbide and air as the main materials. The model is 2D and 3D approximation and the results of the calculation on flow and heat transfer are presented. Thermal and radiation losses are not taken into account. The model has the main objective, model an air solar receiver to achieve the temperature field in the receiver.

The aim of the thesis is to present a description of solar concentration technologies and specifically the solar receiver technology and to present a simplified model for a solar receiver.

Resumo

Numa primeira abordagem, esta tese apresenta um estado da arte sobre as Centrais de Concentração Solar em geral, e posteriormente é feita uma descrição sobre a tecnologia de receptor solar de ar focando-se nas principais características, parâmetros e desenvolvimentos.

Esta tese apresenta também um modelo para um receptor solar de ar de alta temperatura modelado no software de simulação, COMSOL Multiphysics ® usando Carbeto de Silício e ar como os principais materiais. O modelo é uma aproximação em 2D e 3D e os resultados do cálculo de transferência de calor e fluxo são apresentados. Perdas térmicas e radiativas não são tidas em conta. O modelo tem como principal objectivo, modelar um receptor de energia solar de ar de modo a obter o campo de temperaturas no receptor.

O objectivo da tese será de apresentar uma descrição sobre tecnologias de concentração solar e em específico á tecnologia de receptor solar e de apresentar um modelo simplificado de para um receptor solar.

Palavras-chave: estrutura de favo de mel, fluxo de radiação incidente, receptor volumétrico, transferência conjugada de calor, simulação CFD.

Keywords: honeycomb structure, incident radiation heat flux, volumetric air receiver, conjugate heat transfer, CFD simulation.

Index

List of Figures

List of Tables

Nomenclature	**Description**	**Units**
s	Air channel opening	M
L	Air channel length	M
n_{air}	Air flow	$Kmol.s^{-1}$
$c_{p,air}$	Air heat capacity	$kJ.(kmol^{-1}.K^{-1})$
T_{air}	Air temperature	°C
λ_{air}	Air conductivity	$W.(m^{-1}.K^{-1})$
ρ_{air}	Air density	$kmol.m^{-3}$
$A_{cs,air}$	Air channel cross section	m^2
λ_{sol}	Ceramic conductivity	$W.(m^{-1}.K^{-1})$
ρ_{sol}	Ceramic density	$kg.m^{-3}$
$C_{p,sol}$	Ceramic heat capacity	$kJ.(kg^{-1}.K^{-1})$
$A_{cs,sol}$	Ceramic cross section	m^2
T_{sol}	Ceramic Temperature	°C
α	Convection heat transfer coefficient between air and ceramic	$W.(m^{-2}.K^{-1})$
D	Hydraulic diameter	m
u_{air}	Air velocity	$m.s^{-1}$
T_i	Initial temperature	K
αA_v	Volumetric Heat Transfer Coefficient	$W.(m^{-3}.K^{-1})$

Abbreviations

CFD	Computational Fluid Dynamics
CSP	Concentrating solar power
HTF	Heat Transfer Fluid
LFC	Linear Fresnel collectors
CRS	Central Tower Systems
PDC	Parabolic dish collectors
PTC	Parabolic trough collectors
HTM	Heat Transfer Medium
TWF	Thermal Working Fluid
STJ	Solar Tower Jülich
STPP	Solar Thermal Power Plant
DLR	Deutsches Zentrum für Luft- und Raumfahrt
PSA	Plataforma Solar Almería
SSPS	Small Solar Power Systems
ARR	Air Return Ratio
HiTRec	High Temperature Receiver
LEC	Levelised Electricity cost
EPC	Engineering, procurement and construction
O&M	Operation and maintenance
PDE	Partial Differential Equation

1. Introduction

In the past century, the global energy demand has grown and the predictions are that this scenario will increase. Therefore, since 2005, has been a resurgence of concentrating solar power – CSP, mostly due the idea that is a technology capable of large greenhouse gas emission cuts and a sustainable and environmental friendly technology (Lovegrove and Stein 2012).

According to the roadmap (Agency 2010) the growth of CSP electricity production and consumption will increase in each region of the world, see Figure 1 and Figure 2.

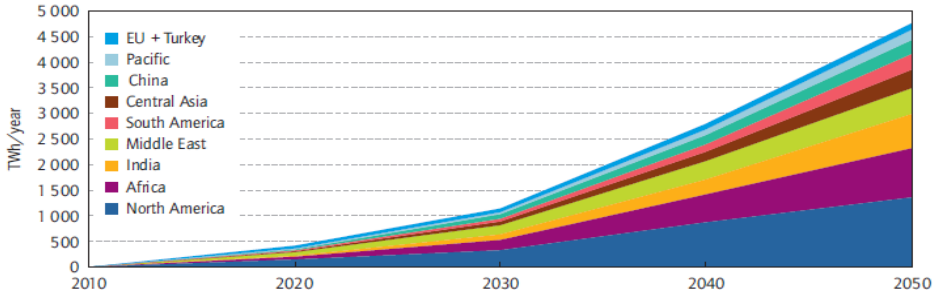

Figure 1 – Growth of CSP production by region (TWh/y) (Lovegrove and Stein 2012).

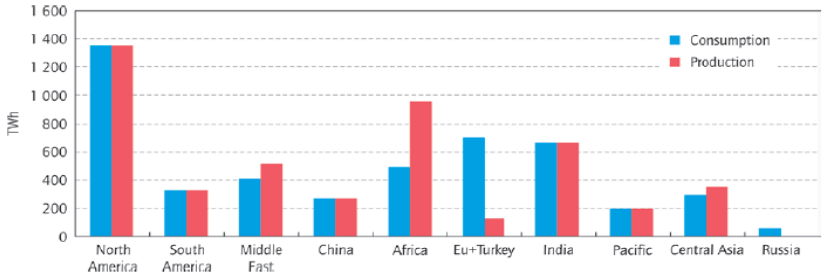

Figure 2 – Production and consumption of CSP electricity by 2050 (TWh) (Lovegrove and Stein 2012).

1.1 Objective

The main objective of this thesis is the development of a model in simulation software of the heat transfer in a volumetric receiver. After a brief introduction, a description of the different solar concentration technologies, general features and operation conditions is made on chapter 2.

This second chapter is followed by a chapter which describes the solar tower technology principle, components and description (chapter 3). A consideration about the receiver concept and types as well as a state of the art of the volumetric air receiver technology is exposed n chapter 4 focusing on history, operating principles and material requirements, specific characteristics and components. In this chapter is also made a brief description of Solar Tower Jülich (STJ). In chapter 5, the theoretical principle about the modulation is made and as a last chapter (chapter 6) the model for the heat transfer and respective results are presented as well as a final chapter (chapter 7) with the most relevant conclusions about the model implemented.

2. Concentrating Solar Power (CSP)

2.1 CSP principles and technologies

Solar energy is an abundant energy source available on Earth, allowing the use of its resources in diverse and varied fields. The use of different technologies to use solar power as an energy source has been growing and reveals high performances thus this energy is an alternative, clean, safe and economic solution to produce cooling, natural lighting, heat and electricity.

Concentrating solar power (CSP) are systems that use combinations of mirrors to concentrate the solar radiation in order to produce electricity. The mirrors (concentrating system) collect the direct sunlight into heat exchangers (solar receiver), where the radiant energy is transferred to a thermal working fluid (TWF) and then, in a thermodynamic cycle this thermal energy is converted into electrical energy (Lovegrove and Stein 2012). The radiation transfer or the fluid transport makes the link between these four main sub-systems. See Figure 3.

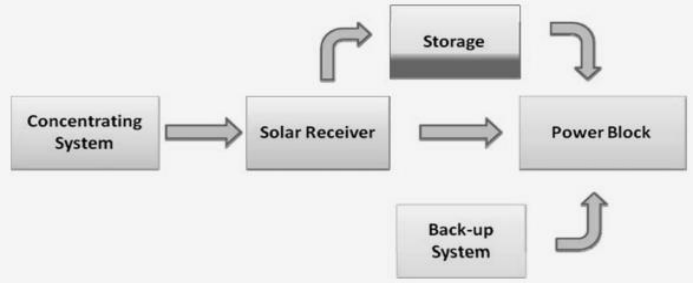

Figure 3 - Main components and sub-systems of a CSP plant including storage (Lovegrove and Stein 2012).

There exist different configurations that are currently used commercially which are:

- Parabolic trough;
- Central receiver tower;
- Linear Fresnel reflectors;
- Parabolic dishes (Lovegrove and Stein 2012).

2.1.1 Parabolic trough

The parabolic trough-shaped mirrors, concentrate sunlight onto a receiver tube along the parabola's focal line. This technology is already commercially available with 1630 MW_{el} in operation and 2130 MW_{el} under construction (Lovegrove and Stein 2012). See Figure 4.

2.1.2 Central receiver tower

Large mirrors with two axis (heliostats) track the sunlight. Then the sunlight is concentrate at the top of the tower where the receiver is. This technology is still at a demonstration stage with 55 MW_{el} in operation and 502 MW_{el} under construction (Lovegrove and Stein 2012). See Figure 4.

2.1.3 Linear Fresnel reflectors

On these systems, the sun's rays are reflected onto stationary receivers which are mounted on a series of small towers facing down, by long rows of flat or slightly curved mirrors. This technology is in a recent phase of development with 10 MWel in operation and 30 MWel under construction (Vogel and Kalb 2010). See Figure 4.

2.1.4 Parabolic Dish

These systems consist in dish systems where the dish has the geometric properties of a parabola but as a three-dimensional paraboloid. The dishes concentrate the direct beam radiation onto a point focus receiver (Lovegrove and Stein 2012). See Figure 4.

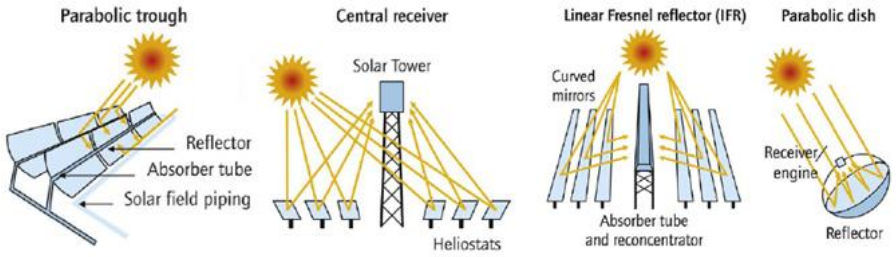

Figure 4 – CSP technologies: Parabolic trough, Central receiver tower, Linear Fresnel reflectors and Parabolic Dish (from left to right) (Agrafiotis, Mavroidis et al. 2007).

Each CSP technology is classified according to the receiver type (fixed or mobile) that is used and the focus type (line or point). Fixed receivers are independent of the plant´s focusing device and stationary devices. These characteristics make easier the transport of collected heat to the power block. Mobile receivers move together with the focusing device. In both line focus and point focus designs, mobile receivers collect more energy. In line focus collectors the tracking of the sun is made along a single axis that focuses irradiance on a linear receiver making tracking the sun simpler. In point focus collectors the sun is track along two axis higher temperatures are allowed due the possibility of focus the irradiance in a single point receiver. See Table 1.

Table 1 - Summary of the different CSP technologies characteristics.

		Focus Type	
		Line focus	Point focus
Receiver type	Fixed	Linear Fresnel	Central Receiver Tower
	Mobile	Parabolic Trough	Parabolic Dish

Depending on how each CSP technology concentrates the solar radiation, the overall efficiency is affected. The parabolic dish is the technology with the best annual optical efficiency (90%) due the axis of the concentrator which is always parallel to the sun's rays. Whit the worst efficiency we have the linear Fresnel system (50%) because of it poor performance in different times of the day (Lovegrove and Stein 2012).

As it was described in the previous section, the CSP systems have different possibilities of configurations concerning the type of system used, the type of heat transfer medium, storage technology, thermodynamic cycle as well as the different configurations for the different components in a CSP plant. An example is given in Figure 5 and Figure 6. In each figure, can be observed a schematic summary of the different configurations and possibilities regarding a component of the CSP technology - the solar receiver system.

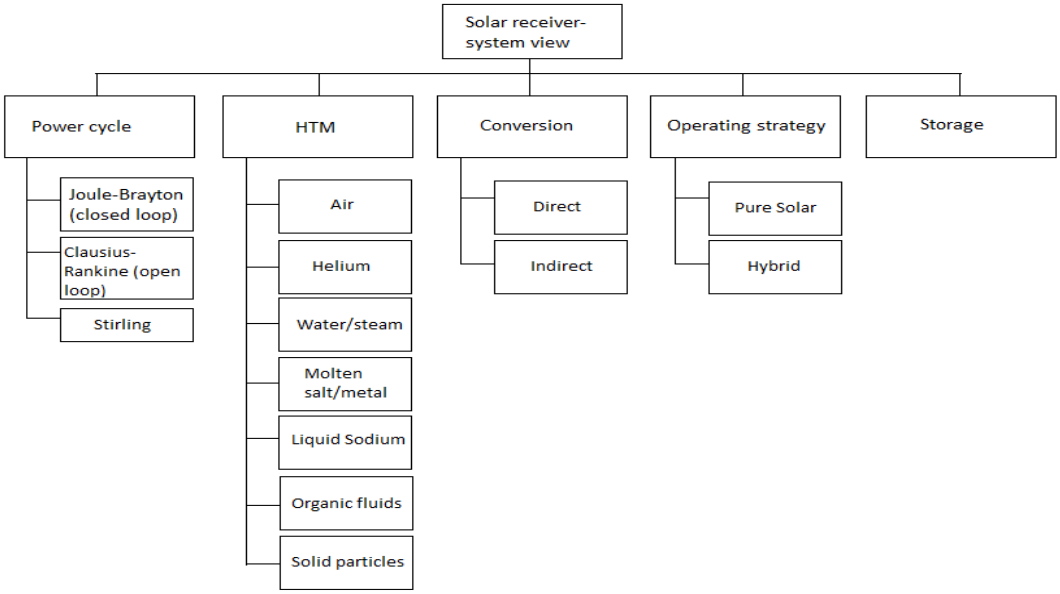

Figure 5 – System view for the solar receiver (Aichmayer 2011).

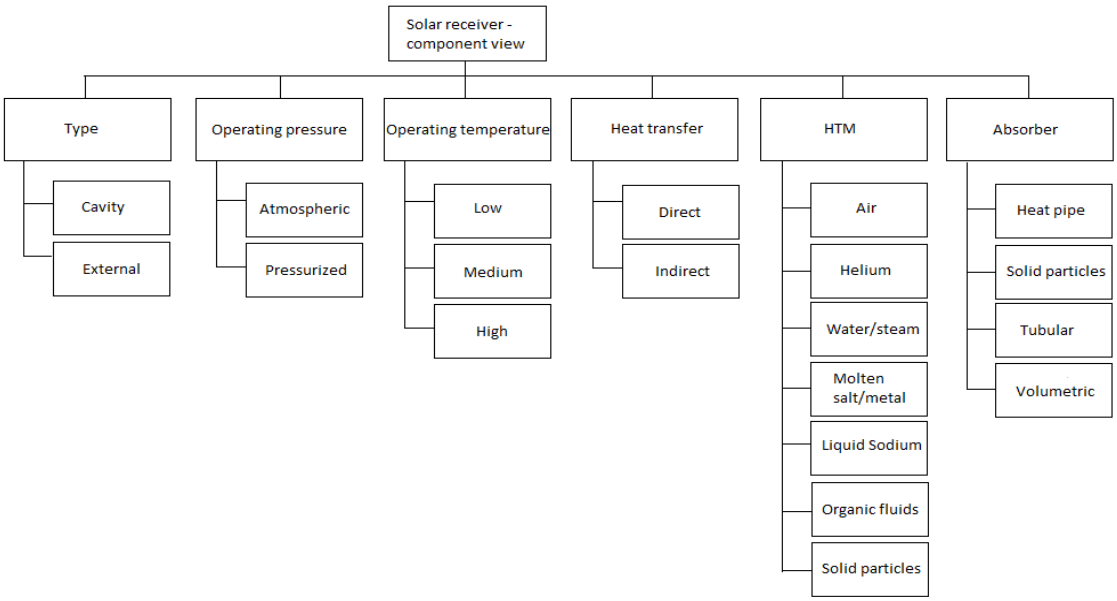

Figure 6 – Component view for the solar receiver (Aichmayer 2011).

Concerning the current performance of these four CSP technologies, the trough plants are already in commercialization and solar tower are making the transition to commercial application. What concerns linear Fresnel and parabolic dishes, these are still in a demonstration stage (Lovegrove and Stein 2012). See Table 2.

Table 2 - Current performance of CSP technologies (Lovegrove and Stein 2012).

CSP technology	**Peak solar to electricity conversion efficiency (%)**	**Annual solar-to-electricity efficiency (%)**
Parabolic troughs	23-27	15-16
Linear Fresnel systems	18-22	8-10
Towers (central receiver systems)	20-27	15-17
Parabolic dishes	20-30	20-25

2.2 Environmental and economic impacts of the CSP technologies

The CSP technologies, like other technologies, are associated with environmental impacts which are described and summarized in the following section.

- Water issues

The water is used in CSP technologies usually at the back-end of the thermal cycle for the cooling process and also for the condensing process. Is often used to clean the mirrors in order to maintain their high reflectivity. In arid areas, this issue is more relevant thus the implementation of CSP in these areas, requires an additional water needs or a different system of cooling (like dry cooling with air) or cleaning with lower water use (Vogel and Kalb 2010) (Fabrizi 2012).

- HTF issues

The leaks or emissions of heat transfer fluid (HTF) can affect components as soil, air or water. These leakages can occur due the absence of insulation during the circulation of the HTF. Systems like parabolic trough, linear Fresnel and parabolic dish technologies, have a higher propensity for leakages since they provide a widespread distribution of the receivers in the solar fields. In systems like the tower system, this issue is less problematic because of the height of the central receiver which can facilitate the dispersion on a large area (Vogel and Kalb 2010) (Fabrizi 2012).

- Land use and visual impact

Land use can be understand as the area directly occupied by a power plant structure and is usually presented in relation to the energy generated annually by each plant (m^2/(MWh/y)). Visual impact respects the area over which a power plant disturbs the view, divided by the energy generated annually by the plant (m^2/ (MWh/y)) (Vogel and Kalb 2010) (Fabrizi 2012). This issue is more critical in the rural landscape where the visual effects are more noticeable (Vogel and Kalb 2010) (Fabrizi 2012). See Table 3.

Table 3 - Land use comparison between energy conversion technologies (Vogel and Kalb 2010) (Fabrizi 2012).

	Land use [m^2/(MWh/y)]	Visual impact [m^2/(MWh/y)]
Parabolic solar power, Spain	11	15
Solar tower power, Spain	24	1100
Photovoltaic power plant, Germany	561	
Wind power	<5	8600
Biomass plantation, France	550	
Open cast mining (lignite), Germany	60	
High voltage power transmission line across Europe	0.4	

- Energy and materials use

What concerns the material used, when compared to conventional fossil-fired plants the CSP technologies are more materials intensive. There are many recyclable materials used in CSP plants as steel, glass and concrete but there are also some non-recyclable materials but most of them are inert thus can be land-filled or used for other things as filling materials. Due the toxicity of the materials used for CSP technologies as the synthetic organic heat transfer fluids soils can be contaminated as well origin other environmental problems. Because of this, these materials are treated as hazardous waste and have been replaced with water or molten salts or other fluids (Vogel and Kalb 2010) (Fabrizi 2012).

[1] Due the fact that photovoltaic power can also be placed on rooftops, this value can be zero corresponding to a zero land use value.

- Emissions

As a green technology, CSP plants have a range of greenhouse gas emission much lower than fossil-fired plants (a difference between 15-20 g CO_2-eq/kWh and 400-1000 g CO_2-eq/kWh) (Vogel and Kalb 2010) (Fabrizi 2012).

- Impacts on flora and fauna

Traffic, building works, ecosystem disturbances and loss of ecosystems are the main local impacts of CSP plants. The surface area of the facility and the type of land use before the construction of the plant are crucial factors respecting the indirect mortality caused by traffic factors, surface treatment on the local fauna and facility construction. Concerning the environmental impacts of the CSP, the most relevant problem is related to the mortality of vertebrates. Deaths occur by collisions with top mirrors and buildings and burning damage or heat shock on the beams of concentrated light. In what respects the flora, the impacts are especially related with places that previously served as agricultural lands with nutrients available in the soil thereby facilitating the proliferation of vegetation that can dry and increase the risk of fire. Comparing these environmental impacts of CSP technology to fossil fuels, the CSP ambient impacts are much lower (Vogel and Kalb 2010) (Fabrizi 2012).

2.3 Economics

A commercial CSP project involves several factors as money and partners. The costs associated as environmental taxes among others are more difficult to quantify. The installation of a CSP plant is expensive although quick when compared with the traditional fossil-fuel plants. It requires a higher capital investment than other energy sources but it also offers long term benefits due it minimum costs of fuel. According to the National Renewable Energy Laboratory, despite these economic facts, CSP technologies can also promote economic growth creating jobs and reducing the cost of energy by reducing the dependence on foreign oil meaning that CSP investment creates more than investments in the same amount of fossil-fuel power (Lovegrove and Stein 2012), (Fabrizi 2012), (Agency 2010), (Coggin 2013) and (Council 2011).

3. Concentrating Solar Power – Solar tower

As it was explained before, solar thermal power plants belong to the point focus systems. In these systems, the direct solar radiation is collected by many heliostats (large mirrored collectors) with a slightly curved glass surface. These surfaces track the sun (two-axis tracking system) so that the reflected solar radiation is intercepted by the receiver. Then the receiver uses this concentrated solar radiation and converts it directly in thermal energy or is transported to another location and then converted (Romero, Buck et al. 2002). Considering that the energy is transported to another location, this transport is made using a heat transfer fluid (HTF) to the thermal storage where is collected and being released at a later time to the power plant process mostly without losses (Research 2013). See Figure 7 and Figure 8.

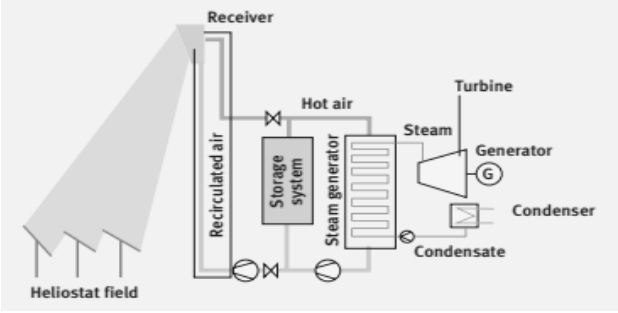

Figure 7 – Plant schematic of a solar tower power plant (Research 2013).

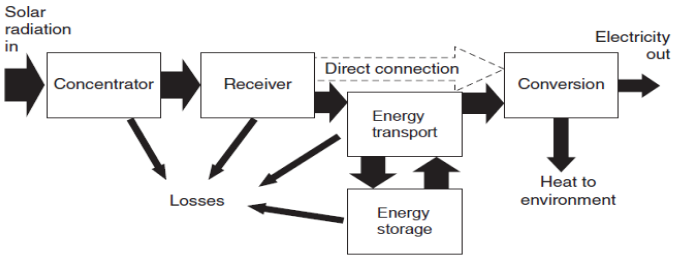

Figure 8 – Process representation of a CSP (Research 2013).

Being a technology with concentrating factors between 600 and 1000 and capable of reach irradiances about 1000 kW/m^2 and 1000 ˚C, the attractiveness of the Solar Thermal Power Plant (STPP) is big since the efficiency of a thermodynamic cycle is proportional to the maximum temperature of the working fluid (WF) giving to the solar tower a long term economic advantage.

The conversion cycles are primarily four differing on the way how solar radiation is concentrated and converted into electricity. Two of these four ways are commercially implemented and the others are still in an experimental stage,

- Pressurized air cycles, experimental, up to 4,6 MW_{el} (e.g. Solugas (SOLAR 2010));
- Atmospheric air cycles, experimental, up to 1,5 MW_{el} (e.g. Jülich (Center 2008));
- Molten salt cycles, 19,9 MW_{el} in commercial operation (Gemasolar (Burgaleta, Arias et al.));
- Direct steam cycles, 31 MW_{el} (PS10 and PS20 (Gonzalez-Aguilar 2007)) in commercial operation.

As it was described before, a solar tower power plant has different elements in it configuration, as the heliostats field, the receiver, the storage system and the power plant.

3.1 Heliostats

Heliostats are mirrored surfaces with a slight curve that use a dual-axis drive operated by an array control system. They use linear and rotary electrical drives or hydraulic actuators for the solar tracking. The size of the heliostats is currently between 1 and 140 m^2. To achieve a desired radiation concentration is necessary that the mirror surface have a high optical quality and precise tracking. The use of calibration methods can minimize the deviations of the systems in the tracking movement (Fabrizi 2012).

3.2 Receiver

The receiver is a key component in a solar tower power plant acting as a heat exchanger (see Figure 9). It is the element of the solar thermal power station which will determine the efficiency of the conversion of solar radiation into heat. The highly concentrated solar radiation is transformed into high temperature heat and then is transferred to the heat transfer medium (HTM) which can be the water or steam, liquid salt and air having the choice of the HTM an influence on the type of receiver (Research 2013).

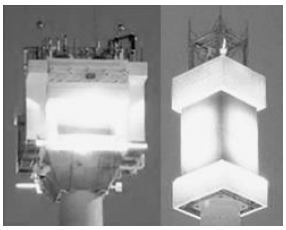

Figure 9 – Cavity and external receiver (left and right) edit from (Gunther).

3.3 Storage system

The storage system is the power plant component where the collected solar heat is absorbed and then released to the power plant process after some time. The type of storage, as the type of receiver, is influenced by the HTM used.

For liquid salt, two tank systems are being used. The liquid salt is heated to 565˚C by the solar energy and then is collected in another storage tank and from here is pumped to the power plant process to generate electricity. In the process, the liquid salt is cooled to 290 ˚C and collected in a second tank and heated up (565 ˚C) again in the receiver if enough solar energy is available. For steam, the steam storage systems are used as a stabilizer system when there are interruptions in the system caused by the occurrence of clouds. Storage systems that use air as the HTM are called as regenerator storage systems. Air flows through the packed bed from top to bottom and the heat is transferred from the air to the storage medium in order to charge the system. When air flows through the storage system in the opposite direction, the system is discharged and the air is heated up (Research 2013).

3.4 Power Plant

Power plants usually use steam processes to generate electricity. The steam processes achieve a thermal efficiency of 42% according to the system and HTM used. Solar-heated gas turbine systems and or recuperative gas turbine systems are good alternatives to the steam processes having a higher efficiencies (Research 2013).

4. Receiver

The function of the receiver is absorb the concentrated solar radiation energy coming from the heliostats field and transfers it to the thermal working fluid (TWF). The receiver concept is usually divided in cavity or external receivers or cylindrical or flat receivers. The dimensions of the receiver are also an important fact having it influence in the optical efficiency of the receiver.

The following sub-section will give a short information about the shape and aperture of the central receiver independently of the equipment used (silicon carbide pipes, ceramic foam honey-comb modules, wire mesh, secondary concentrator, or quartz window) and from the heat transfer fluid used (water, molten salt, atmospheric air, or pressurized air). Also a general description about the receiver concept performance will be taken in consideration.

4.1 Receiver types

4.1.1 Cavity/external receiver and cylindrical/flat receiver

Cavity receivers (Figure 9) are receivers where the absorber surface is protected, i.e., is concave or disposed within a cavity. Therefore, it is protected from the atmosphere in all directions except that of the heliostats field and has a circular or rectangular window shape in the top of the tower in order to reduce the radiation and convection losses to the atmosphere (Xu 2013). External solar receivers (Figure 10) are receivers where the solar absorbing surface is on the outside of the structure, i.e., the side surface (cylindrical surface) is the surface which absorbs solar radiation. The external receivers have no protection and thus are prone to wind cooling and radiation losses to the sky (Harris and Lenz 1985).

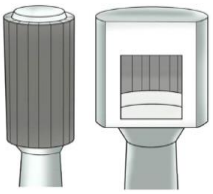

Figure 10 - Cavity and external receivers (right and left) (Ho and Iverson 2014).

4.2 Receiver dimensions and performance

The width or the diameter and the height give us the overall dimensions for the receiver. The dimensions of the receiver strongly influence the final optical efficiency due the spillage losses (when the reflected light misses the target). If the receiver is smaller than the heliostats field, is necessary to increase the heliostats canting. Even if the receiver is larger as the heliostats field, there is always the necessity of focusing heliostats with curved mirror and canting although to a lesser extent.

In an energy balance of a receiver at steady state, the net energy will be a balance between the energy outflows from the flow of heat transfer fluid and energy losses. The losses in a central receiver are due mainly to the following heat loss types: reflection, radiation, convection and conduction (Lovegrove and Stein 2012).

$$\dot{Q}_{loss} = \dot{Q}_{refl} + \dot{Q}_{rad} + \dot{Q}_{conv} + \dot{Q}_{cond} \tag{1}$$

The energy performance of the central receiver is the ability to convert the incident concentrated radiation into heat power carried by the heat transfer fluid (Lovegrove and Stein 2012).

$$\eta_{rec} = \frac{\dot{Q}_{converted}}{\dot{Q}_{input}} = \frac{\dot{Q}_{input} - \dot{Q}_{loss}}{\dot{Q}_{input}} \tag{2}$$

Where for the receiver (Lovegrove and Stein 2012)

$$\dot{Q}_{input} = \int_{time} \int_{aperture} G_{incident}(t) dA dt \quad (3)$$

4.2.1 Radiative and refection losses

The radiation losses depend on the materials emissivity according to the Stefan Boltzmann Law applied to a real surface. The total normal emissivity of silicon carbide is close to 90% of a blackbody for a temperature between 500˚C and 1000˚C. Depending on the receiver temperature and emissivity radiation losses can represent more than 50% of the total receiver losses (Winter, Sizmann et al. 1991)

The reflectivity losses are based in the reflectivity factor and its complementary absorption factor of the receiver materials. The total reflectivity of the receivers made of ceramic, may exceed a 10% total reflectivity above 500˚C without selective coating and drop down to 5% with coating. Depending on the receiver technology, the total receiver losses can reach 30% (Winter, Sizmann et al. 1991).

This way the radiative loss process includes the radiation emitted from the receiver and the reflection of a portion of the concentrated solar radiation. Taking into account a simplified model and a general receiver, the radiation losses and reflection losses are given by the following equations (Lovegrove and Stein 2012).

$$\dot{Q}_{rad} = \sigma A F_{RS} (T_{rec}^4 - T_{amb}^4) \quad (4)$$

$$\dot{Q}_{refl} = (1 - \alpha) A \dot{Q}_{sol} \quad (5)$$

Where F_{RS} is the shape factor between the receiver and the surroundings.

4.2.2 Convection losses and conduction losses

The convective losses are a result of the movement of the air over hot receiver surfaces. The convection losses are dependent on the ambient atmospheric temperature and the wind velocity and the receiver shape and are often close to a quarter of the total receiver losses (Lovegrove and Stein 2012).

$$\dot{Q}_{conv} = hA(T_{rec} - T_{amb}) \quad (6)$$

The conduction losses will be due the material and paths between hot receiver surfaces and the environmental depending on geometry and material conductivities (Lovegrove and Stein 2012).

$$\dot{Q}_{cond} = \frac{T_{rec} - T_{env}}{R_{th}} \quad (7)$$

4.3 High temperature solar central receivers

In this sub-section information about the general principle and review of previous modelling and testing activities, expected outlet temperature and thermal efficiency, benefits and research needs of the high temperature central receivers will be provide.

4.3.1 Gas receivers - small particle air receivers, tubular gas receivers and volumetric air receivers

4.3.1.1 Small particle air receivers

In this type of gas receiver (which first concept appeared in 1970s), the suspended particles (submicron carbon particles) absorb the radiant energy in a pressurized cavity air-receiver. The energy

is then transferred to the HTF (air) for high-temperature gas-turbine (Brayton cycles) where the thermal energy is converted into electricity. There are multiple advantages of the use of this type of heat exchangers as,

- High incident fluxes with no solid absorber that can be damage and high temperatures because the absorbers are expendable;
- Due the large cumulative surface area of the particles, the solar radiation is absorbed throughout the gas volume → higher efficiencies;
- Minimization of the reradiation of the thermal energy and maximization of the incoming light due the optical properties of the particles;
- No resistance to heat transfer because the particles are at thermal equilibrium with the surrounding;
- Minimization of the pressure drops by removing the tubes and foam absorbers (Hunt 2012), (Ho and Iverson 2014), (Miller and Hunt 2012) and (Flamant, Gauthier et al. 2014).

Based on studies, the receiver efficiency can reach values up to 90% depending on some parameters as, particle concentration and size, mass flow rate, temperature and optical properties of the window and particles.

What respects the outlet temperature of the air, conducted experiences showed that small-particle receivers can reach the value of 700 ˚C. There are some aspects around this type of receiver that need an improvement as,

- Development of a suitable window;
- Development of a solid-gas suspension system capable of maintain a desired particle concentration and temperature within the receiver.

(Miller and Koenigsdorff 1991), (Miller and Koenigsdorff 2000) and (Abdelrahman, Fumeaux et al. 1979).

4.3.1.2 Tubular gas receiver

Since 1970s that this concept exists and experimental tests and prototypes have been carried on until this days. The first developments of this type of receiver were made for parabolic dish receivers and liquid-metal heat tubes were used in order to achieve higher levels of heat transfer from the concentrated solar radiation to the thermal working fluid (gas). Since the internal heat transfer coefficient for liquid metal pipes it is much bigger than heat transfer coefficient for heat transfer to gas some advantages can be linked to the liquid-metal pipes technology,

- Ability of tolerate higher solar fluxes;
- Compact receivers;
- Lower metal temperatures;
- Lower pressure drops.

Recent developments about this receiver concept carried by Deutsches Zentrum für Luft- und Raumfahrt (Research), showed an increase of the thermal efficiency from 68% to 81%, and a reduction of the convective and radiative heat losses and possible hybridization. Possible improvements can be done in different aspects of the receiver and in new receiver concepts and designs.

- Efficiency improvements about the use of the window;
- Issues related with the large convective and radiative heat losses associated to this high temperature receivers, the difficulty of transferring the heat in an effective way to the irradiated tubes which affect also the durability of the receiver;

- Study of flux limits;
- Study developments about the use of the sCO2 as a HTF for CSP systems due the possibilities of attain higher efficiencies (above 50%) (Ho and Iverson 2014).

4.3.1.3 Volumetric air receivers

The operating principle of this type of receiver is the following one, the concentrated sunlight irradiates the porous structure (as honeycombs or porous ceramics) and at the same time, air flows through the porous structure and is heated up to temperatures that varies with the material used. For metals, the air can reach temperatures between 800 ˚C and 1000 ˚C, for ceramics temperatures up to 1200 ˚C and up to 1500 ˚C for silicon carbide. After this process, the air is used to heat the working fluid, charge the storage medium and/or pass to the gas turbine. See Table 4.

Table 4 - Air temperatures respecting the material used (Ávila-Marín 2011).

Structure material	Outlet Air temperatures
Metal	800 ˚C - 1000 ˚C
Ceramics (SiSiC)	>1200 ˚C
Silicon carbide (Multiphysics)	>1500 ˚C

Since the 1980s that this technology is being developed but only in 1991s some results of experiments were reported. In this first stage of the technology the peak mean outlet air temperature was about 730 ˚C and the peak flux for the absorber was greater than 800kW/m^2. After some problems related with the optimization of the design, high radiative heat losses, efficiency and outlet air temperatures, other concepts of this technology were conceived in order to solve them.

- A two-slab selective volumetric receiver (semi-transparent multilayer) system: decreasing of radiative heat loss;
- A similar concept employing square glass channels: improvement of the efficiency;
- Use of a volumetric solar receiver employing ceramic pins (“Porcupine”): showed the capability to achieve higher gas temperatures (1000 ˚C).

4.3.2 Liquid receivers – tubular liquid receivers and falling-film receivers

4.3.2.1 Tubular liquid receivers

This type of receiver has the following working principle, an array of thin-walled tubes made of stainless steel or other materials. These thin-walled tubes are arranged in order to transport the working fluid through the incident solar radiation. This technology has been studied since 1970s but only in the 1980s and 1990s the technology was implemented. Several studies has been carried on concerning different uses of HTF, optimization of designs to achieve less significant reradiation effects, improvements on the efficiency and temperatures achieved.

4.3.2.1 Falling-film receivers

This technology consists in a working fluid that falls down through a wall and is directly irradiated by the sunlight or is heated up by the wall. This characteristic allows less pumping requirement. Studies regarding a maximization of the efficiency, film stability, heat losses reduction, design improvements to a bigger fluid control among others issues have been carried until the present.

4.3.3 Solid particle receivers

In solid particle receiver, the concentrated solar radiation heats up the solid particles (sand) which are falling through the cavity of the receiver. After being heated, these solid particles are used to heat a secondary working fluid (WF) for the power cycle or before this, stored in an insulated tank.

This concept came out in the 1980s and has been in development since then. The main objective is to improve the outlet temperature of the receiver up to 1000 ˚C using the capability of store the solid particles. Therefore several studies and experiments have been carried out concerning different aspects of the solid particle receivers as,

- Increase the particles temperature: recirculation;
- Increase the thermal efficiency: decreasing the radiation and convective losses;
- Improvements on solid particles properties

4.4 Volumetric Air Receiver Technology

4.4.1 Historical approach

The first tests about this type of receivers were reported in 1970s in United States of America (USA) by a company called SANDERS Assoc. and Pacific North West Laboratory of Battelle. After some tests about large storage capacity of molten salt plants as a HTF, the activities about this receiver were shifted to Europe (during the 1980s) having the focus in the development of volumetric receivers using air as HTF.

The studies in Europe were initiated by the study for a Solar Thermal Power Plant in the Maroz Valley in Switzerland (SOTEL) where the metal wire mesh receiver was developed, built by the SULZER-company and tested on the Plataforma Solar de Almeria (PSA). Meanwhile, another concept about the volumetric receiver (Volumetric Foil Receiver) was introduced in Atlanta and Winterthur during the SSPS meetings (1995 and 1986). The development of ceramic volumetric receivers began when DLR adopted the ceramic foil concept, after some feasibility studies. The studies about this concept continue until today to improve some aspects related for example with the absorber durability, the specific cost and the efficiency of the receiver (Hoffschmidt, Téllez et al. 2003), (Singh, Saini et al. 2010) and (Spelling, Favrat et al. 2012).

4.4.2 Operating principles

The receiver is located on the top of the solar tower and works as a heat exchanger, i.e. it converts the solar radiation into thermal energy that is later converted into electricity. The conversion of the solar energy to thermal energy is made using a heat transfer medium as it was discussed in the previous section (salt, air, water/steam or liquid/metal). Also the geometry of the receiver can change depending on the concept/configuration see Figure 11.

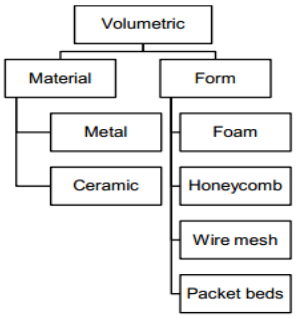

Figure 11 - Classification of volumetric solar receivers (Aichmayer 2011).

Atmospheric air cycles are based on an open loop where the ambient air is drawn through a volumetric receiver made of wire mesh or porous ceramic foam installed inside of the a volume in the receiver (Hoffschmidt, Téllez et al. 2003), (Hoffschmidt, Pitz-Paal et al. 1999).

The solar radiation is absorbed in the depth of this structure heating up the material and at the same time, the air (TWF) passes through the volume being heated up (680-950°C) by forced convection and the radiation and then is converted into thermal energy. The process continues with the WF being directed either through a packed bed storage unit typically made of rocks (Singh, Saini et al. 2010) (during charge), or through a steam generator driving a conventional steam cycle (during discharge). Subsequently the return air is blown back to the receiver inlet, and a share of it is drawn again into the loop (ARR: Air Return Ratio, e.g. 45%). Other atmospheric air cycles as pure solar combined cycle with an air-air heat-exchanger were proposed in order to replace the combustion chamber (Spelling, Favrat et al. 2012).

4.4.3 Specific characteristics – volumetric effect and flow stability – and advantages

There are two main characteristics of the volumetric receivers that characterize the volumetric effect, see Figure 12. One of them is the high absorptivity of the porous structure which allows the absorption of the concentrated radiation in the interior of the receiver. The other one is that the effective area for solar absorption is many times larger than that of thermal radiation losses (Romero, Buck et al. 2002).

Other characteristics can be seen as an advantages of the volumetric receivers like the simplicity of heat transfer mechanisms which reduces the material stresses and the outlet temperatures of the air it is higher. Also higher solar fluxes in the receiver aperture are allowed due the large absorption surface reducing in this way the receiver size (Hoffschmidt, Téllez et al. 2003).

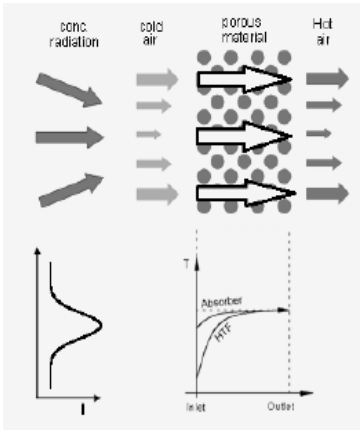

Figure 12 - Heat transfer principle in open volumetric receiver: typical distribution of the incoming solar radiation across the aperture (left), material and air temperature distribution perpendicular to the -aperture and along the direction of air flow (middle) edit from (Fend, Hoffschmidt et al. 2004).

The flow stability is an important issue when dealing with volumetric receivers. The pressure between the two sides of the sample is what determines the mass flow density, see Figure 13.

Figure 13 - Schematic representation of the consequences of a pressure drop in the volumetric receiver.

Unstable gas flow leads to local overheating, poor performance and local failures (melting and cracking). The most influent parameter on the flow stability is the pressure loss of the porous media. According to Darcy flow, the pressure drop within the porous media depends linearly on the flow velocity thus instability can occur.

$$\frac{dp}{dx} = \frac{\mu}{K_1}.\vartheta + \frac{\rho}{K_2}\vartheta^2 \quad (8)$$

p is related to the pressure, x the coordinate in the direction of the flow, K_1 and K_2 the viscous permeability coefficient and inertial permeability coefficient respectively (absorber characteristics), μ dynamical viscosity, ρ the density and ϑ the fluid velocity.

The advantages of the volumetric air receivers are multiple contributing for a higher efficiency of the thermodynamic cycles (around 75% or even more) as well as what concerns other point of views.

- High system efficiency: the steam turbine process can be operated with the high steam parameters in the same way as a conventional power station;
- Environmental compatibility: the air and water are the only carriers and WF used in an air receiver technology which are free and fully available providing high safety levels and protection; these two elements are also non- toxic;
- Reliability and hybridisation: major parts of the plant can be built using standard components from conventional power plant construction; the plant concept can be expanded by adding an additional furnace making possible simple hybrid operation;
- Power availability: the constant fluctuations in production can be avoid due the possibility of adapt the plant's energy production to the demand by having a hot gas storage unit;
- Others: no risk of freezing, simpler system, fast response to transients or changes in incident flux, no special safety requisites, no environmental impact (Romero-Alvarez and Zarza 2007), (Karni, Kribus et al. 1997) and (Becker, Fend et al. 2006).

4.4.4 Basic structure

The receiver, as a large structure of the solar tower follows the concept of a modular concept, which means that the receiver is sub divided into sub receivers. Inside of those sub receivers there are the absorbers (Figure 14).

- Absorber modules

Ceramic absorber which direct the air flow, each one with an individual fixed orifice so the air mass flow rate distribution can be adjusted to a design flux density distribution.

- Sub-receivers

It is the part of the receiver where the airflow of the modules is split. The controllable air flaps installed on the sub receivers are used to control the overall mass flow rate of each sub receiver.

The controllable air flaps are able to adapt the sub receiver air mass flow rates and temperatures such that the combination of the sub receiver air mass flow rates results in a total flow with desired receiver air outlet temperature, see Figure 14.

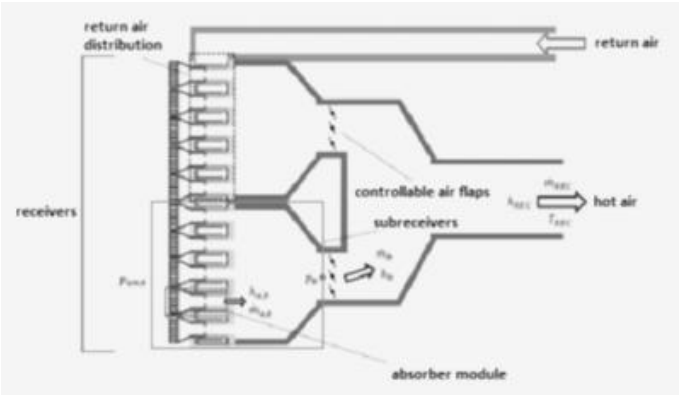

Figure 14 – Volumetric receiver structures and details (Ahlbrink, Andersson et al. 2013).

4.4.5 Material requirements

There are some basic requirements that the absorber material has to accomplish concerning optical and thermodynamics aspects, see Table 5.

Table 5 - Optical, thermodynamic and resulting material requirements of absorber materials (Scheffler and Colombo 2006).

Optical/Thermodynamic requirements	Material requirements
High absorption	Dark
Optical extinction	High porosity
Heat transfer surface	High cell density
High flux	Temperature resistance
Radial heat transport	Thermal conductivity
High permeability	3D structure

The performance of the receiver is affected by some parameters as flux density and it distribution on the receiver, the air mass flow and it distribution on the absorbers.

Higher the open porosity, higher the quantity of radiation that penetrates into the structure contributing for high quality volumetric absorbers. The convective heat transfer is a parameter that depends also on the structure, thinner the structures (wires, walls) better the convective heat transfer. A good volumetric absorber is characterized by the volumetric effect meaning that the absorber temperature at the irradiated side is lower than the temperature of the medium leaving the absorber.

The mass flow distribution can show instabilities under specific operating conditions of the volumetric absorber. Receiver arrangements with mass flow adaptation elements located behind the absorber can reduce this tendency, as well as appropriate selection of the operating conditions and the absorber material (Palero, Romero et al. 2008). Other properties of the volumetric air receiver can affect it the performance,

- Geometric properties: mean cell size, porosity and the shape of the strut cross-section;
- Optical properties: absorptivity, extinction coefficient and scattering phase function;
- Thermo physical properties: thermal conductivity and thermal capacity of ceramic foam materials;
- Fluid properties (Wu, Caliot et al. 2011)

The extinction coefficient, absorption coefficient and scattering coefficient can be explained considering spectral radiation of intensity I_λ (s, Ω) incident on a volume element of length along the direction of propagation s. After propagation in the medium, some amount of energy can be lost due to absorption and/or out- scattering. The decrease in radiation is given as,

$$dI_\lambda(s,\Omega) = -\beta_\lambda(s) I_\lambda(s,\Omega) ds \quad (9)$$

Where β_λ is called the spectral extinction or attenuation coefficient of the. The unit of β_λ is [m^{-1}] and depends on the local properties of the medium (temperature, pressure among others). The extinction coefficient consists of two parts and is given by the following equation,

$$\beta_\lambda = k_\lambda + \sigma_{s,\lambda} \quad (10)$$

Where k_λ is the absorption coefficient and $\sigma_{s,\lambda}$ is the scattering coefficient. Both parameters have also a unit of [m^{-1}] and they are called volumetric coefficients. The absorption coefficient describes how radiative energy is converted to internal energy of the matter. Therefore it couples the radiative energy propagation with the thermodynamic state of matter. On the other hand, out-scattering is the change of the direction of radiation propagating along s. Scattering means that no radiative energy is converted to thermal energy.

In a non-participating medium, β_λ is zero and there is no change in intensity as it propagates along the path. Table 6 it is a summary of the volumetric air receiver characteristics (Siegel and Howell 2002).

Table 6 - Volumetric air receiver characteristics (Menigault, Flamant et al. 1991)

Receiver design	Outlet temperature/thermal efficiency	Benefits	Challenges/Research needs
Volumetric air receiver	> 700˚C/50-60%	Capable of achieving high temperatures, simple and flexible construction	Material durability, flow instability, radiative heat loss, low thermal efficiency, long term storage

4.5 The High Temperature Receiver (HiTRec) – Ceramic Open Volumetric Air Receiver

4.5.1 Beginning of the technology

This technology first appeared in 1995 and 1996, during the tests comparison of different available ceramic absorber materials in the solar furnace at DLR. The tests demonstrated that the most satisfactory materials for the absorber were the Silicon Carbide or Silicon infiltrated Silicon Carbide (SiSiC) particularly an extruded honeycomb SiC structure, see Figure 15. These structures showed the best results respecting thermal shock, temperature and flow stability (Fernandez, Konstandopoulos et al.).

At the same time, it was found that on high heat flux, highly porous materials proved to have unstable air flow through the absorber structure. This fact affects the absorber because it leads to cracking or melting of the absorber structure by local overheating. The high temperature solar receivers arose when it was found that it was not possible to use absorber materials with a high potential of thermal efficiency due the possibility of destruction due to flow instability. In this way, the flow stability and thermal efficiency were two factors taken into account and the development of receivers and absorber materials was divided (Hoffschmidt, Téllez et al. 2003). The high temperature solar receiver is a structure where the front is formed by a set of ceramic absorber modules and the back part is composed by a stainless steel structure. Due to the possibility of thermal expansion of the modules or the movement of the structure of stainless steel, each absorber module is fixed from the back. The fact that the modules are separated by a gap, contributes to use the return air from the waste heat recovery boiler to feed the front of the structure and to an easier replacement of the absorber modules. Despite this characteristics and developments, the high temperature solar receiver is not directly associated to a specific absorber material having the possibility of be placed in metallic or ceramic cups (Hoffschmidt, Pitz-Paal et al.).

4.5.2 Development from 1997 until the present days

After the development and manufacture (1997) of HiTRec, this technology was tested in the PSA in Spain until 1998. One of the first aspects to be considered in the development of high-temperature receiver was the use of ambient air to cool the steel structure extending the durability of the system operating at temperatures above 1000˚C the output. The results were satisfactory,

- The receiver achieved maximum outlet temperatures around 980 ˚C and demonstrated easy operability including the absorber;
- Good thermal efficiency of 75% at 800 ˚C average outlet temperatures when compared with previous ceramic receivers; (Hoffschmidt, Pitz-Paal et al.).

The problems with this type of volumetric receiver were related with the stainless steel structure which has been deformed due an error design of the air cooling system. In 1998, in order to achieve a solution for this problem, a new concept for the HITRec was developed by Ciemat, Inanbensa and DLR – HiTRec II (Ávila-Marín 2011). The results were,

- The durability of the stainless steel was demonstrated thus the main goal was accomplished;
- The materials of the absorber modules were replaced for monoliths leading to a overheat and the necessity of changing the modules;
- The thermal efficiency achieved was inferior of the last HiTRec version (HiTRec I) due the impossibility of measure precisely the flux and due the overheating of the side areas of the absorber modules.

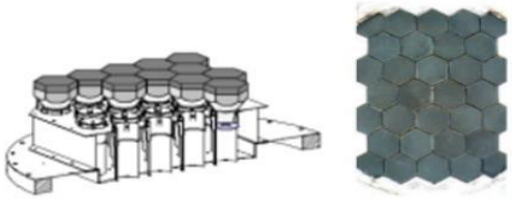

Figure 15 – Cut (left) and front view (right) of the HiTRec II receiver (Hoffschmidt, Pitz-Paal et al.).

Current developments have been made around this technology as the development of a modular solar geometry of these receptors in order to facilitate the replacement of damaged absorber modules and to include a return path for air to re-use the hot air from the boiler and to cool down the structure.

One of the other many objectives is to reach a homogeneous temperature on the back part of the modules. Therefore, tests including measurements of temperature and thermal trace maps have been made in order to determine ways to reduce thermal gradients from behind the absorber cups.

4.5.3 Absorber developments

As already mentioned, the HiTRec is not intrinsically linked to a type of absorber structure, being possible to use different materials for the absorber modules than the ceramic and allowing the individual development of the absorbers.

Since 1994 more than 15 types were studied by DLR up to today with the main goal to resolve the instability of the flow and select the most appropriate materials and structures (Hoffschmidt, Pitz-Paal et al.). On Table 7 the different absorber materials investigated along the years are presented. A general description about the place, materials investigated and company/institute and main parameters is made. In Figure 16 is possible to see the different materials for the absorber structure.

Table 7 - Investigated porous materials (Fend 2010).

Materials investigated	**Identity**	**Place**	**Parameters**
IKTS foam ceramics	Institut für Keramische Technologien und Sinterwerkstoffe	Dresden, Germany	Cordierite, λ_{wall}≈1 W/mK Siliconised silicon carbide, SSiC, λ_{wall}≈100 W/mK Clay bound silicon carbide, CBSiC, λ_{wall}≈10 W/mK
SiC fibre mesh	Schott Glas	Mainz, Germany	Silicon carbide fibres of 25 µm diameter 3.5 mm thickness fibres oriented in directions perpendicular to the direction of the air flow
Ceramic (Multiphysics) catalyst carriers	HELIOTECH	Denmark	Channel width of 2 mm Wall thickness of 0.8 mm excellent resistance to high temperatures up to 1600°C
Metallic catalyst carriers	EMITEC	Germany	800 and 1600 cpsi (cells per square inch)

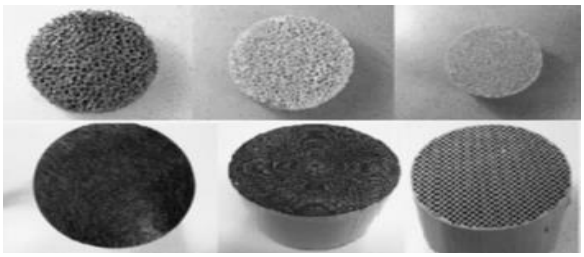

Figure 16 - Ceramic foam manufactured by the IKTS on top and catalyst carrier materials (silicon carbide fibre mesh, metallic and silicon carbide from left to right) (Fend, Hoffschmidt et al. 2004).

4.6 Solar Tower Jülich (STJ)

The construction of the solar tower Jülich (STJ) was completed in 1998. The type of receiver uses the same principle as the HiTRec, having air as the HTF and working exclusively with solar energy providing electricity to the grid. The solar tower capacity in Jülich is 1.5MW. When was built, its main purpose was to support the idea that this type of concentrating solar technology was viable and to serve as a reference to future projects.

4.6.1 Receiver at STJ

The type of receiver used in the solar receiver Jülich solar tower is a HiTRec similar to that previously described in chapter 4.5. The use of this solar receiver is justified by the fact that it enables a high potential of the solar tower due to the high temperatures reached therefore achiving high thermodynamic conversion efficiencies. In tube solar receivers, the higher temperatures are achieved on the wall structure and not on the HTF therefore the heat transfer efficiency is affected and even more when, like in this situation, the HTF is the air.

Because of this and due the fact that this solar receiver in STJ is a volumetric air receiver, the absorption of concentrated solar radiation takes place inside the porous structure and the structure is simultaneously cooled by ambient air flowing inside the receiver. Therefore, the front of the receiver remains at a temperature lower than the HTF (volumetric effect). In this way, the receiver used in STJ is a volumetric air receiver of high temperatures with a porous structure with flow channels as an absorber. The material used for the absorber is ceramic, specificly Silicon Carbide, due the possibility of achieve higher gas outlet temperatures because of it high thermal conductivity.

In Figure 17, a shematic representation of the receiver can be observed. The back part of the solar receiver is constituted by a stainless steel structure that supports the set of modules of ceramic absorbers constituting the base of the receiver.The absorber modules are separated by a space allowing its movement and thermal expansion so dramatically shortened the possibility of contact between modules. The base of the support structure is a membrane capable of double sheet cooled by ambient air flowing from the exterior to the interior of the receiver or by the return air from the boiler.

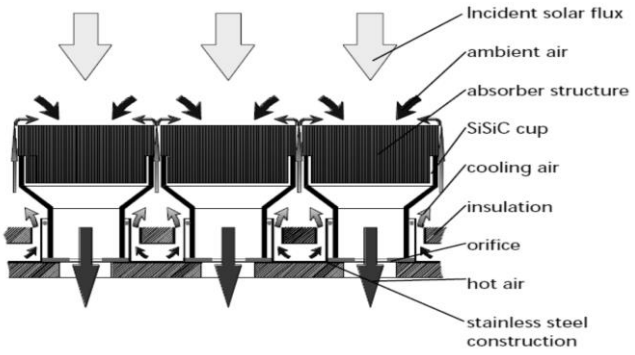

Figure 17 – Receiver structure and basic process (Hirsch, Ahlbrink et al. 2012)

The absorbers cups have attached pipes which passes in front of the membrane sheet through orifices and are welded to the bottom sheet of the double layer membrane. This double layer membrane is cooled by the air circulating in the receiver which also cools down the sides of the structure as it circulates by the absorbers segments.

The air reaches the front of the absorbers through the space between them. The air getting inside the structure and the air from the boiler are mixed together and re-sucked into the structure of the absorbers. As penetrate into the absorbent structure, the air is heated by convection. When exits the absorber structure, the hot air is conducted to the bottom part of the cup. According to the solar flux simulations, an orifice is sized adjusting the mass flow rate of air compensating the solar flux profile in the aperture achieving a homogeneous outlet temperature. The orifices determine the air flow distribution and the return air. The receiver design is fully modular. Due this fact is possible to scale the power levels by multiplying the basic sub-units as is shown in Figure 18.

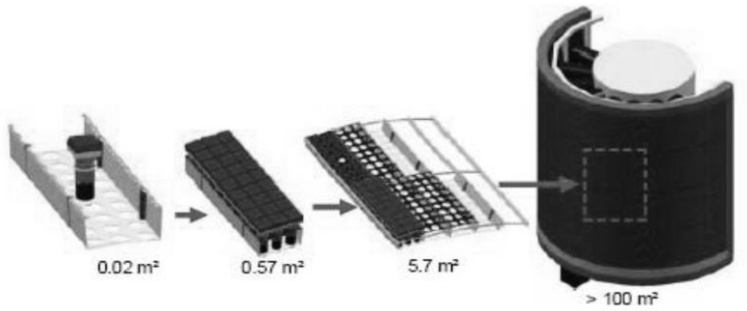

Figure 18 – Volumetric air receiver modular concept (Hennecke, Schwarzbözl et al. 2009).

4.6.2 Design, engineering and erection

About 2150 heliostats with 8m^2 of reflective surface form the concentrator field of the Solar Tower Jülich. The heliostats are densely packed in rows on an area of about 8 ha and are designed with a single back-silvered glass facet fixed to a metal frame. Due to its small size, the use of a simple linear drive unit to track the sun is possible (Hennecke, Schwarzbözl et al. 2009). Many ceramic absorber modules, like the ones described in chapter 4.5 in sub section 4.5.3, make part of the receiver The tower has 60m height and the receiver is mounted on it top having an aperture facing down of 25º.

The air is sucked and heated up by the receiver until 700ºC in the primary cycle and then used to generate steam in a heating tube boiler. The boiler delivers live steam at 480°C and 27bar. The steam drives a turbine of 1500kW electric design power. The thermal storage system is situated in the primary cycle parallel to the boiler. The storage system consists of large vessel filled with porous ceramic bricks. The storage is charged through the hot air which passes through the large vessel from top to bottom heating up the storage material.

Therefore, a thermo cline zone is developed between the hot and cold ends of the storage. The air flow from the cold end of the boiler and or from the storage is returned to the receiver with a temperature of about 100ºC proceeding to the charge of the storage. The discharge happens when the cold airs from the steam generator is circulated in reverse flow from bottom to the top through the storage vessel and back to the steam generator, see Figure 19. The entire plant is installed in the tower except the dry cooling system which is located outside of the tower (Hennecke, Schwarzbözl et al. 2009).

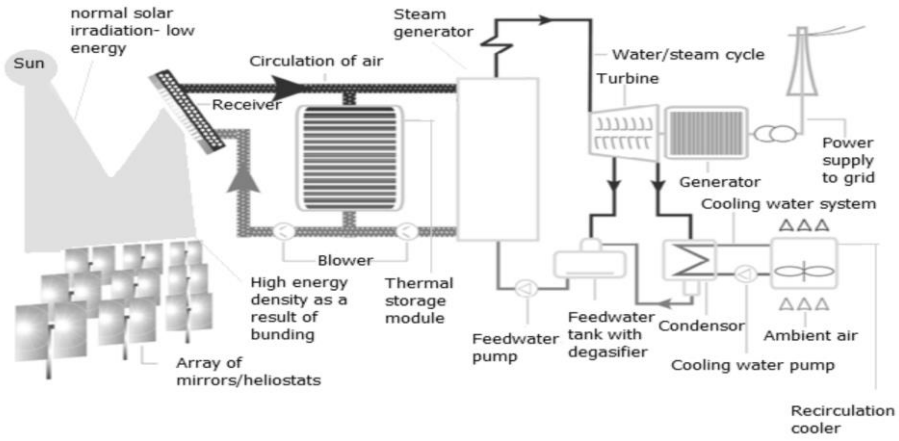

Figure 19 – Principle of the solar towe power plant Jülich (Koll 2011).

4.6.1 Construction phase, start-up and operation

The construction of the STJ began in 2006 with the phase of detailed engineering and acquisition of major components. The physical construction began in 2008 after solving bureaucratic factors being the receiver mounted in the month of November of this same year. The end of the construction of the STJ was in 2008 when the absorber elements were installed in the receiver structure. The start-up and operation carried out in the STJ is summarized in Table 8.

Table 8 - Solar tower power plant project phases.

Start up	End of 2008
Heliostats calibration	Autumn 2008
Receiver operation	Beginning of 2009
First solar electricity delivered	April 2009
R&D programm	End of 2010

5. Theoretical model

The current model describes the thermal performance of one single channel in the receiver and has been investigated numerically. The receiver system works like a thermal heat exchanger between the fluid phase and the solid phase therefore the model describes the air flow and heat transfer in the receiver channel.

To describe the temperature distribution of the solid and the fluid, partial differential equations are needed therefore energy balance for fluid and solid, respectively, are used.

$$\rho_{fluid} \cdot c_{p,fluid} \cdot u_{fluid} \cdot \left(\frac{\partial T_{fluid}}{\partial x}\right) = k_{fluid} \cdot \left(\frac{\partial T_{solid}}{\partial x}\right) + \alpha \cdot A_v \cdot (T_{solid} - T_{fluid}) \quad (11)$$

$$\rho_{solid} \cdot c_{p,solid} \cdot \left(\frac{\partial T_{solid}}{\partial t}\right) - k_{solid} \cdot \left(\frac{\partial T_{solid}}{\partial x}\right) = \alpha . A_v \cdot (T_{solid} - T_{fluid}) \quad (12)$$

Some assumptions were made which are exposed in the next topics.

- Fluid flow inside the system is horizontal, from the inlet to the outlet;
- The fluid thermo physical properties are temperature dependent;
- The system is insulated therefore, heat losses to and from the surroundings are neglected;
- Steady-state condition, i.e. operate with constant fluid temperature at the inlet and within the receiver channel independent of time;
- Uniform distribution of fluid and solid temperature;
- The flow velocity and temperature at the inlet is uniform over the flow cross section.
- The fluid flow rate is uniformly distributed through the receiver.

In COMSOL Multiphysics, in order to conjugate the heat transfer in the fluid and solid, the mathematical formulation used for the steady state and laminar flow was the Navier-Stockes equation and the energy conservation. In a stationary state, the controlling parameters are defined as numerical constants and the model is allowed to converge at the equilibrium state defined by the specified constants, therefore since we want to obtain a final outlet temperature value with no time-varying loads, the option "Stationary study" was selected in the model builder.

As already referred, the main objective of this model is to simulate the temperature distribution of the fluid (air) along the receiver structure obtaining a final outlet temperature, therefore, being a fluid subject to a temperature change (the expectation is that air at 150ºC heats up until around 700ºC), its material properties, change accordingly. The changes can have an influence on the flow field depending on how large are the changes; the temperature is also affected by changes in the flow field due the fact that fluid transports heat, therefore, in the simulation was considered a non-isothermal flow because is two-way to couple heat transfer and fluid flow.

The modules and respective differential equations used in COMSOL Multiphysics are provided above.

- Weakly compressible Navier-Stockes: Navier-Stokes equation, the energy conservation law and the equation of continuity

$$\rho(v.\nabla)v = \nabla.[-pI + \mu(\nabla v + (\nabla v)^T) - \frac{2}{3}\mu(\nabla . v)I] + F \quad (13)$$

$$\frac{d\rho}{dt} + \nabla.\rho V = 0 \quad (14)$$

Since we are assuming a steady-state the continuity equation is expressed as;

$$\frac{d\rho}{dt} = 0 \Rightarrow \nabla . \rho V = 0 \tag{15}$$

In each equation, V is the velocity field [m/s], p the pressure [Pa], F the forces acting on the volume [N/m], ρ the fluid density [kg/s], μ the dynamic viscosity [Pa.S], ∇ the vector differential operator and I the identity matrix.

- Convection and heat conduction in air

$$\rho . C_p . u . \nabla \mathrm{T} = \nabla . (\mathrm{k} \nabla \mathrm{T}) + \mathrm{Q} \tag{16}$$

$$q_0 = \alpha A_v (T_2 - T) \tag{17}$$

Where T is the temperature [K], k the fluid thermal conductivity [W/m^2], Q the heat source [W/m^3], C_p the heat capacity [J/(kg.K)] and ∇T the temperature gradient.

- Heat conduction in the solid

$$\rho . C_p \frac{dT}{dt} - \nabla . (\mathrm{k} . \nabla T_2) = \mathrm{Q} \tag{18}$$

Since this is a steady state problem which means that the temperature does not change with time, the first term of equation (16) disappears.

$$-\nabla . (\mathrm{k} . \nabla T_2) = \mathrm{Q} \tag{19}$$

Where k is the thermal conductivity k. The energy exchange between the solid and fluid phase is made through the volumetric solid-to-fluid heat transfer by convection.

$$q_0 = \alpha A_v (T_2 - \mathrm{T}) \tag{20}$$

By solving two heat transfer equations, is possible to calculate two different temperatures in the channel of the receiver, one for solid phase and another one for fluid phase.

6. Mathematical model

6.1 Introduction

The receiver model is implemented in COMSOL Multiphysics®, simulation software that will be discussed through this chapter. As it was explained in section 4.6, the system studied here is similar to the one in the solar tower Jülich where the heat transfer fluid is the air and the receiver structure is the silicon carbide.

The model has as objective the simulation of the stationary state of the thermal interaction between air and solar volumetric air receiver structure when air is passing through the solid part. Only a single channel of one honeycomb structure is simulated and the mesh used is the one designated by COMSOL Multiphysics as "Normal" in order to reduce the computation time (this time is indicated by the software and using this mesh is faster to achieve a solution due the faster convergence). Since no heat losses are considered, the same conditions are assumed for each parallel channel so that all the channels will have a similar behavior.

6.1.1 Overview of the COMSOL Multiphysics application Modes – version 4.2

Through the simulation is possible to design and predict quality and posterior reactions and improvements about the design avoiding errors and mistakes in posteriors phases as the manufacturing phase. COMSOL is a multiphysics and single physics simulation which covers electrical, mechanical, fluid and chemical simulations, based on advanced modelling and simulating problems in physics-based numerical methods. This software offers the possibility of multiphysics and couple phenomena, including and coupling all relevant physical effects, see Figure 20. Since is necessary to couple different phenomena in the simulation the multiphysics characteristic (availability of couple two or more physics that affect each other) that the software provides is crucial (Multiphysics 2013).

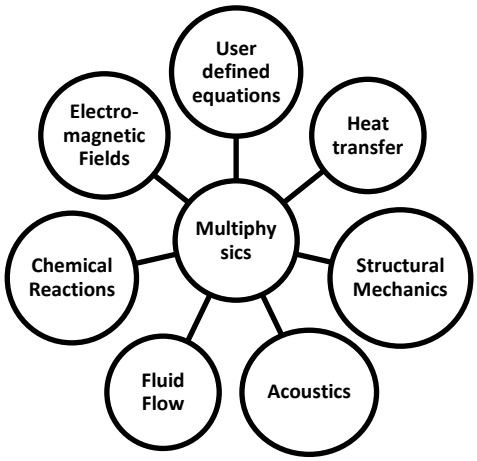

Figure 20 – Multiphysics approach (COMSOL).

6.2 Receiver system general properties

The receiver system installed in STJ is a HiTRec receiver type, where air circulates through the receiver acting as a HTF and the concentrated solar radiation heats up the ceramic honeycomb material.

The receiver installed in STJ is an open volumetric air receiver with flow channels with an aperture of 22,7 m^2 and several ceramic absorber modules. The system operates between 150°C and 700°C (Hennecke, Schwarzbözl et al. 2009) with a mass flow of 12,1 kg/s , see Table 9. The air flows from the inlet to the outlet of the system being in direct contact with the receiver structure. The air flow keeps flowing in this direction.

Table 9 - Receiver specific characteristics.

Receiver Specifications	
Temperature range	150-700°C
Mass Flow	12,1 kg/s
Aperture area	22,7 m^2

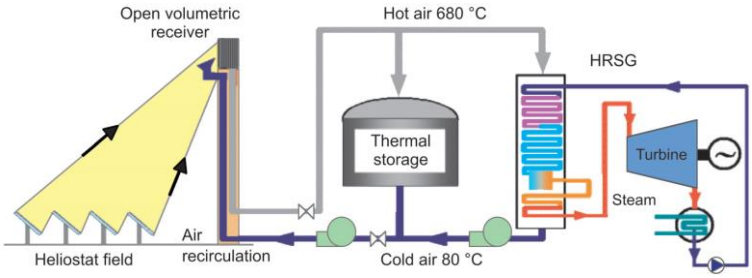

Figure 21 - Flow chart of a steam turbine driven by solar tower technology.

The system works according to the principle in Figure 21. The air flows through the hot ceramic elements (heated up by solar radiation) which form the receiver, heating up the air around 700ºC. According to (Agrafiotis, Mavroidis et al. 2007), using ceramic honeycombs is possible to have thin walls and high geometric surface area therefore higher temperatures can be tolerated. The honeycomb structure is made of silicon carbide which is the solid phase as it shown in Figure 22. Air is the fluid phase.

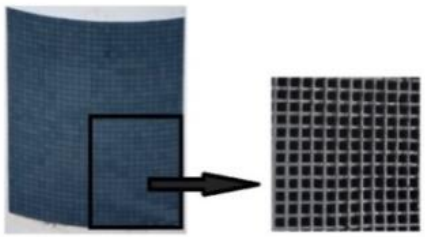

Figure 22 – Honeycomb structure.

The receiver structure material used is silicon carbide. Its thermo physical properties are in Table 10.

Table 10 - Silicon carbide properties.

Silicon carbide	
Channel dimensions	2x2x30 mm
Thermal conductivity	120 $W/m^{-1}.K^{-1}$
Heat Capacity	0,670 J/g.ºC
Density	3100 k g/m^3

6.3 Physical Model

In Figure 23 can be seen the physical model in 2D. The physical model consists of a quadrangular channel with length L=30 mm and a width of T=0,4 mm, and an opening s=2 mm. During the heating process, heated air flows through the channel and a temperature gradient is achieved during this process.

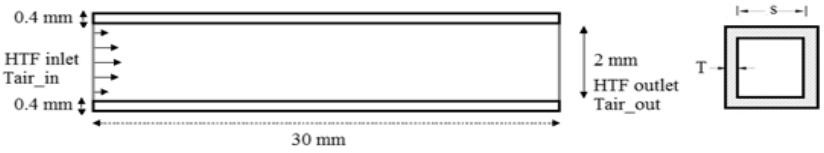

Figure 23 - Physical model of the volumetric receiver single channel.

The channel is discretized in a certain amount of points, between 0 and L. During the process, the channel is heated up by an incident flux [W/m^2] and the cold air flows through the channel from the inlet to the outlet. During the process, a temperature gradient is achieved where $T_{fluid\ outlet} > T_{fluid\ inlet}$. Figure 24 shows a representative scheme of the temperature distribution on the receiver.

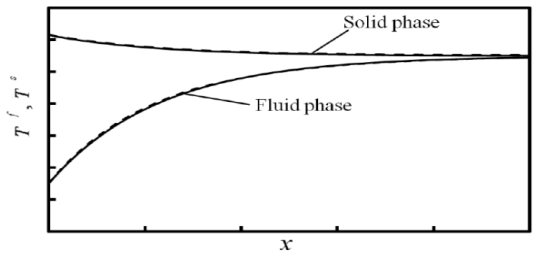

Figure 24 – Typical variations of fluid and solid temperatures (Honeycombs: axial) (Sano and Iwase).

For the fluid, the air inlet temperature is constant and the system is in equilibrium when the fluid temperature equals the solid temperature.

$$T(0) = T_{air,inlet} \tag{21}$$

6.4 COMSOL Considerations

6.4.1 Physics modes

COMSOL Multiphysics provides a number of application modes that consist of predefined templates and user interfaces with equations and variables for specific areas of physics but is also possible to establish our own PDE-Partial Differential Equations due the three PDE modes that COMSOL Multiphysics provides.

For the simulation, was used the physics modes that COMSOL Multiphysics provides meaning that the software computes the PDE coefficients based on application-specific parameters and material properties. Working with a physics mode it is possible to access settings for material properties and boundary conditions among others (Multiphysics 2013). The COMSOL modules used were the weakly compressible Navier Stockes, conduction in the solid and convection and heat conduction in the air, see chapter 5.

6.4.2 Solver

In 3D modelling, the memory issue is more crucial than in other modelling geometries. To facilitate this process, COMSOL chooses the more suitable solver to our problem by a default choice. Since the problem is a steady state case, the solvers used were the stationary solvers more specific the PARDISO and MUMPS solvers. These solvers are used by default since they make use of available disk space to solve large models that do not fit in the available memory (Multiphysics 2013).

6.4.3 Mesh

The mesh features enables the discretization of the model geometry into various elements of the mesh (smaller units of simple shapes). Model results are directly related to the mesh used. Accordingly to the mesh used, a more accurate solution and better convergence of the model will be attained.

Comsol multiphysics by default create triangles/tetrahedral that are as isotropic as possible (non-flat), a large number of elements will be created in a thin layer. Also, large differences in scale may cause the mesh generator to fail in creating the mesh. In what concerns the choice of the appropriate mesh there is different element types. There are four different 3D element types – tets, bricks, prisms and pyramids, see Figure 25.

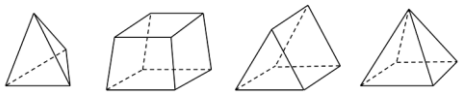

Figure 25 - Different element types for linear static finite element problems (Multiphysics 2013).

To mesh any model in 3D, this four elements can be used, in various combinations and for 2D models, there is triangular and quadrilateral elements available.

Having less than 5-10% changes in results indicate that a proper mesh is being used, i.e., too much changes indicates a too coarse mesh, too small changes might indicate a very fine mesh. Making a mesh to fine will not have visible changes in the results, the only problem is when the mesh is too fine, the RAM limit might be hit or it would solve very slowly (Multiphysics 2013). The meshes available are designated by COMSOL Multiphysics as extremely fine, extra fine, finer, fine, normal, coarse, coarser, extra coarse and extremely coarse. The type of mesh that was used in the 3D simulation was created using COMSOL's physics based meshing option; this mesh is designated by COMSOL Multiphysics® to be Normal, see Table 11 and Figure 26.

In order to check if the changes where between 5-10%, the mesh was changed using a fine mesh and a coarse mesh despite the normal mesh. This way, the simulation in 3D was studied for fine, normal and coarse mesh in Figure 26. The changes obtained were about 10% therefore, a crucial parameter in the selection of the mesh was the computation time. In a coarse mesh the simulation took around 5-10 minutes running, when a normal mesh was used it took 15-20 minutes running and when a fine mesh was used the simulation took around 30-40 minutes running. Another simulation using finer meshes (extremely fine, extra fine, and finer) was discarded to present here due computation time higher than this one presented here. See Table 11.

Table 11 - Elements specification for each mesh studied.

	Fine Mesh	Normal Mesh	Coarse Mesh
Domain elements	805000	326736	145650
Boundary elements	88840	43988	27768
Edge elements	2288	1620	1284

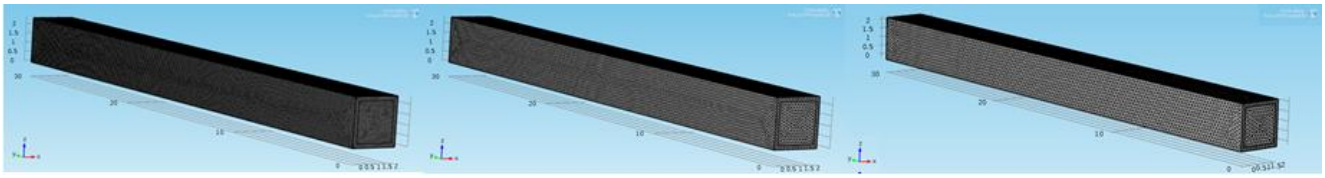

Figure 26 – Fine, normal and coarse meshes (from left to right).

This way, the mesh used was a normal mesh for both geometries (2D and 3D).

6.4.4 Space selection, geometry and material domains

When performing a computational fluid dynamics is necessary to have a good geometric model so a 2D and 3D space selection was made and the geometry was built using the features of COMSOL Multiphysics®. The first geometry in 2D consists in tree rectangular features; see Figure 27 and the second geometry consists in 2 blocks (an inner block and an outer block) see Figure 28.

- Rectangle 1: 2 mm height and 30 mm length;
- Rectangle 2 and 3: 0,4 mm height and 30 mm length.

The second geometry consists in two 3D blocks with the respective dimensions, Figure 28.

- Inner block: 2, 0 x 2, 0 mm with 30 mm length;
- Outer block: 2, 8 x 2, 8 mm with 30 mm length.

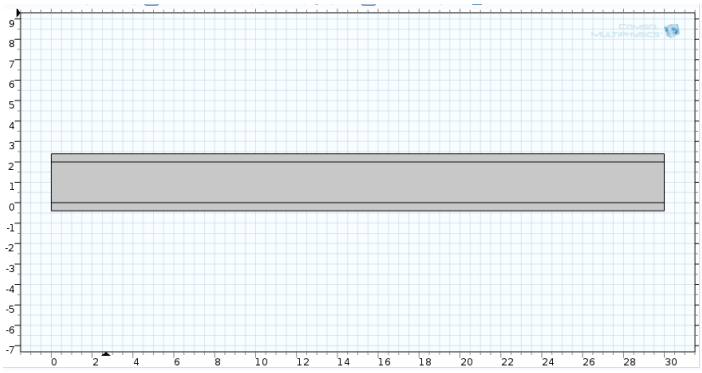

Figure 27 – 2D geometry.

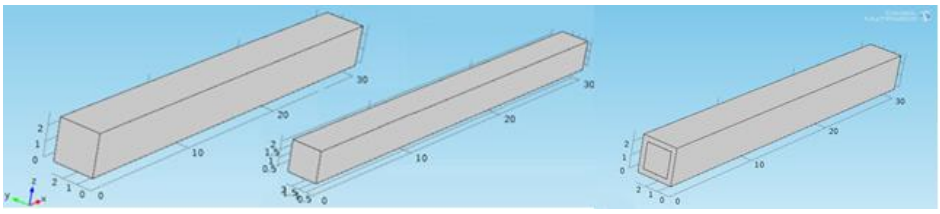

Figure 28 – Outer and inner blocks and complete 3D channel geometry (from left to right).

Each material is represented usually the temperature and the SI units (International System of Units) is used to describe the properties. This way, by selecting for the solid part the SiC from the material library available in the software and air for the fluid phase, the respective properties are available in the library. These properties are based in different references available in the software. The silicon carbide properties applied are shown in Table 10 and the air thermo physical properties are temperature dependent. The respective domains for each material (air and SiC) are shown in Figure 29.

Figure 29 – Air and SiC domains respectively (from left to right)

6.4.5 Boundary conditions

The solution of the temperatures depends on the physical conditions existing at the boundaries of the system. This way the boundary conditions to solve the problem are exposed in this next section.

- Thermal insulation: this boundary condition ensures that there is no heat flux across the boundaries meaning that the temperature across the boundary is zero, see Figure 30. This way the system is well insulated.

$$-n.(-k\nabla \mathrm{T}) = 0 \tag{22}$$

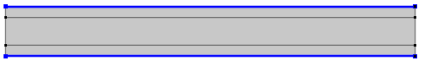

Figure 30 – Thermal insulation.

- Initial values: this node is added to the model by default. Table 12 show the initial conditions input in the software.

Table 12 - Input initial conditions.

Velocity	Pressure	Temperature
(0, 0) m/s	0 Pa	20°C

- Inlet

In this node, a set of boundary condition as velocity, pressure, no viscous stress and normal stress or mass flow is included which described the fluid flow at the entry point, i.e., at the entry of the channel (see Figure 31). The boundary condition used for the inlet condition was the mass flow.

Figure 31 - Inlet boundary.

The value of the total mass flow of the receiver as well as the total area of the receiver is known as it can be observed in Table 13.

Table 13 - Conditions specifications.

Total mass flow [kg/s]	12,1
Air density (atmospheric pressure and 150ºC) [kg/m^3]	0,8342
Total area [m^2]	22,7

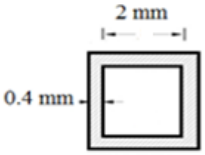

Figure 32 – Single channel dimensions.

To calculate the mass flows for each channel were used these values as well as the dimensions of each individual channel. Knowing the total area of the receiver and the area of each single channel, the number of channels was calculated and then the total mass flow was divided for the total number of channels. This way the mas flow per channel used as an inlet condition was 4,18 x 10^{-6} kg/s.

- Temperature

This node is used in order to specify the temperature in a certain point in the geometry, see Figure 33 and Table 14, and can be on the boundaries or surfaces. The equation for the temperature is

$$T = T_0 \tag{23}$$

Where T_0 is the temperature that the inlet boundary is subject.

Figure 33 - Temperature condition and boundary in the inlet (fluid and solid, left and right).

Table 14 - Inlet conditions.

Inlet Temperature Fluid	Inlet Temperature Solid	Inlet mass flow
150 [˚C]	800 [˚C]	4,18 x 10^{-6} [kg/s]

- Outflow

This boundary condition was used mainly because in our model the details of the flow velocity and pressure at the outlet are not known prior to solution of the flow problem. This way the outflow node provides a suitable boundary condition for convection dominated heat transfer at outlet boundaries and is used to model flow exits where the details of the flow velocity and pressure are not known prior to solution of the flow problem as it happens in this model. Any condition is defined in the outflow boundary.

This condition states that only heat transfer over boundary is by convection. The temperature gradient in the normal direction is zero and there is no radiation. This describes a good approximation of the conditions at the outlet in this case, heat transfer model with fluid flow. The fluid and heat transfer simulation was set by the input of the variables for the fluid flow and heat transfer properties for the fluid and solid parts and temperatures for the inlet and walls of the channel. The temperatures of the walls were set with a higher value than the inlet temperature of the fluid flow. For the 3D geometry the boundary conditions input were the same.

6.5 Results

The HiTRec module consists of two phases, a fluid and a solid phase, see Figure 34.

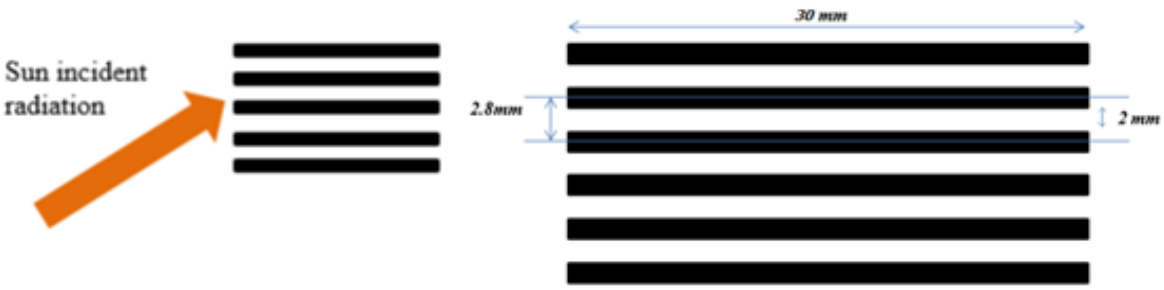

Figure 34 – Incident concentrated sun radiation on a HiTRec solar receiver module and channels distribution (left and right respectively).

The fluid phase as already said is the air and it can be considered as a transparent medium because it has no effect on the radiation due to its very low absorptivity. In order for the ray to penetrate inside the channel walls, the radiation intensity has to be incident with an inclination angle with the normal to the inlet or else part of the ray will pass through the transparent medium from the inlet to the outlet without any absorption. The study of the radiation was analysed in 2D geometry and divided in three parts.

6.5.1 Heat flux along the total length of the channel

On a first approach, to study the radiation on the channel, an incident heat flux along the inner upper wall of the channel was considered meaning that the concentrated heat flux was treated as wall heat flux boundary condition during the thermal analysis. See Figure 35.

For the simulation of the temperature on the solid part, the physics heat transfer in solid only in the solid body was used and the following boundary conditions were set. A temperature condition in the front surface of the channel was prescribed (as the initial temperature of the front face of the solid body).

The next step was input a heat flux of 800 kW/m^2 on the inner upper wall of the channel in order to simulate a incident radiation with a certain angle since in COMSOL Multiphysics ® is not possible to prescribe an angle and direction to a heat flux. Since the incident heat flux in the front of the receiver is between 600 kW/m^2 and 1100 kW/m^2, was considered that the incident flux in the inner wall is 800 kW/m^2. A general heat flux q_0 is used to add heat flux across boundaries. Was selected the respective boundaries for the heat flux and the respective value according to the data supplied, see Figure 35.

Figure 35 - Layout of the incident radiation on the channel wall and boundary heat flux in COMSOL.

$$q_0 = 800\ kW/m^2 \tag{24}$$

The solution for the temperature in the solid body is presented below. Due to the input heat flux, simulated by the temperature along the upper inner wall, the solid body temperature raises up from the inlet to the outlet (around 6000ºC). The lower wall has no variation of its temperature along the channel since there is no input condition of energy as in the upper wall.

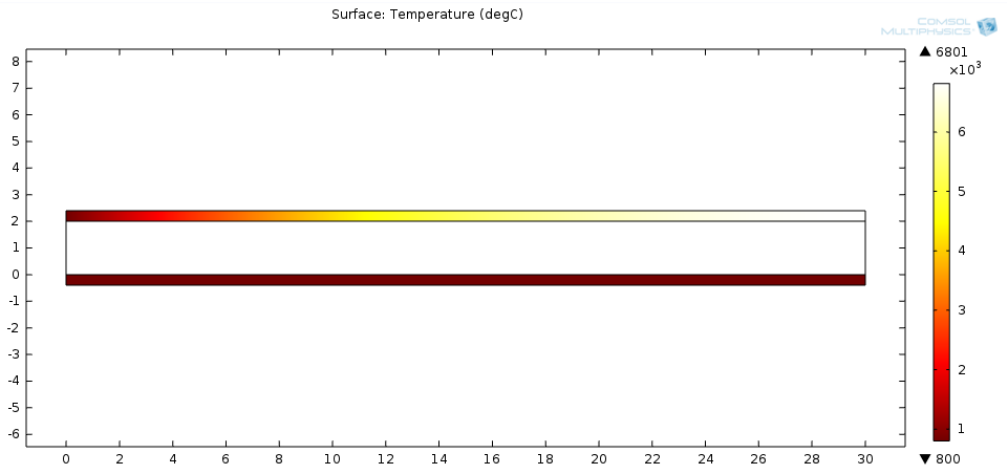

Figure 36 – Temperature distributions in the solid body.

This temperature distribution on the solid body, see Figure 36, was then used to simulate the temperature distribution on the model with fluid flow and solid together. To do this, the temperature distribution of the solid part was used on the non-isothermal flow model as a volumetric heat source only where the heat flux has an effect therefore the physics, "Heat transfer in solids" and "Non-isothermal flow" was coupled.

For the volumetric heat source, a value of volumetric heat transfer coefficient used was 50000 W/m^3/K according to previous works in SIJ. This way, it is assumed that the radiation works as heat source and warms up the structure and a working fluid (air) passes through the channel and cools it by convection (heat sink). The radiation energy is transformed to thermal energy.

The heat source term (heating power per unit volume) for the solid part was,

$$Q = \alpha A_v (T_F - T_S) \tag{25}$$

Applying this solution in the non-isothermal flow model, the temperature of the fluid and solid phases are demonstrated in Table 15 and Figure 37 shows the temperature values obtained in the outlet of the channel. The values were taken in the outlet of the channel where the black line in the figure is.

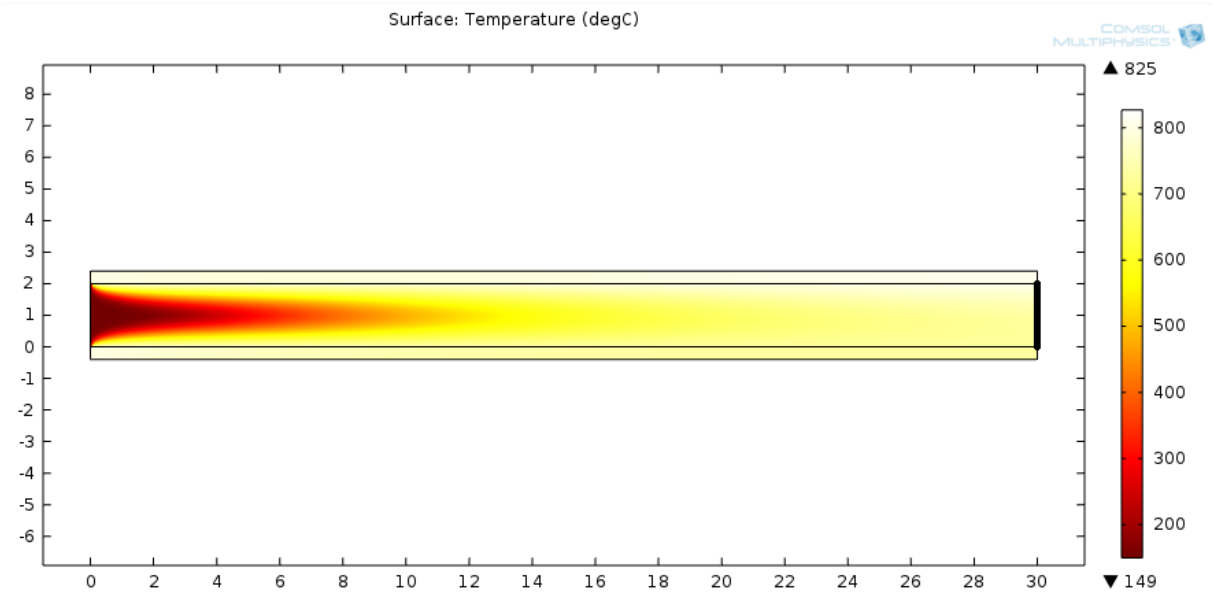

Figure 37 - Temperature distribution.

Table 15 - Temperature values on the outlet of the channel with respect to the fluid phase.

Average Temperature in the Outlet (˚C)	Maximum Temperature in the Outlet (˚C)	Minimum Temperature in the Outlet (˚C)
744,02	805,70	721,62
Average temperature of the fluid in the channel (˚C)		
620,59		

Along the outlet of the channel, the temperature varies according to the following chart in Figure 38.

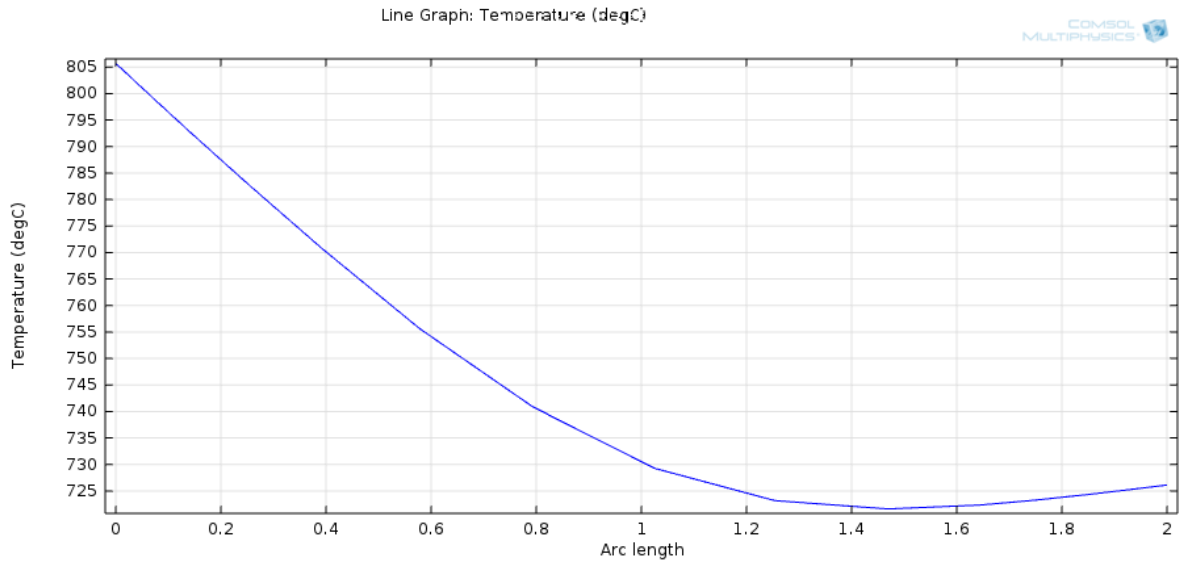

Figure 38 – Chart representing the temperature distribution of the fluid along the outlet.

Since the upper wall on the outlet has a higher temperature, T=805,70 °C (due the heat flux condition applied on the boundary solid-fluid) than the lower wall, T=721,62 °C, the fluid temperature is warmer near the upper wall and decreases as it approaches the bottom wall. The chart below in Figure 39 shows the temperature distribution along the channel respecting the fluid and solid phase.

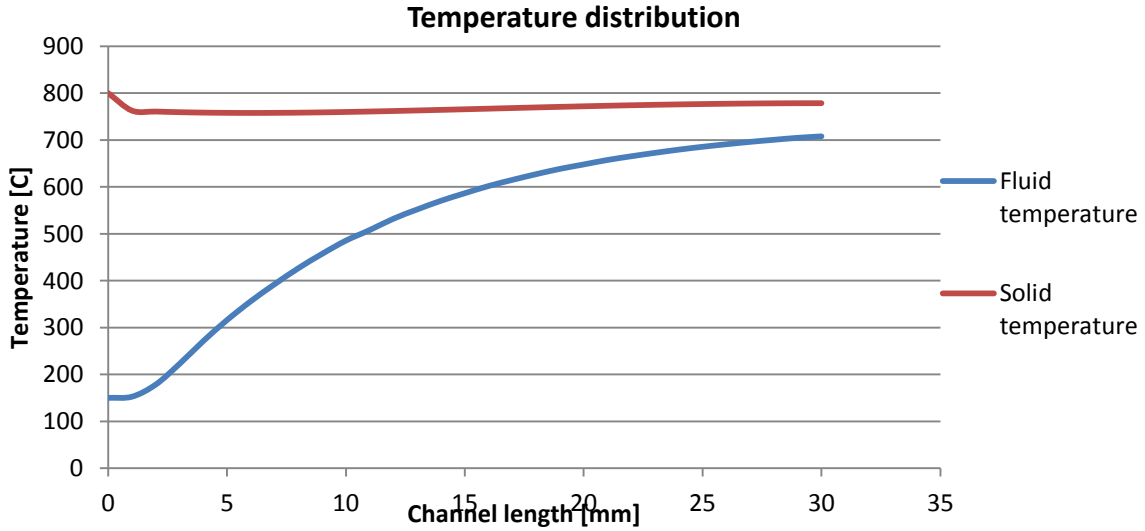

Figure 39 – Fluid and solid temperature distribution along the channel.

6.5.2 Heat flux along half of the length of the channel

In this second approach, a more realistic situation was considered, meaning that the concentrated solar radiation has only an effect in the first half of the channel (L/2=15 mm), see Figure 40 and Figure 41.

Figure 40 - Heat flux prescribed only in the first half of the channel.

The methodology used was the same as the previous simulation, first the temperature distribution was solved only for the solid body, Figure 42, and after the solution for the solid body was imported to the model where fluid and solid phases are interacting together, see Figure 43.

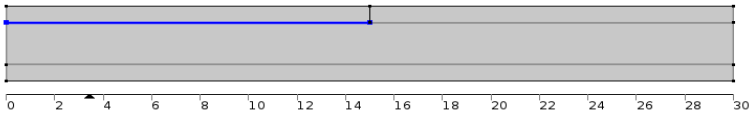

Figure 41 – Prescribed heat flux.

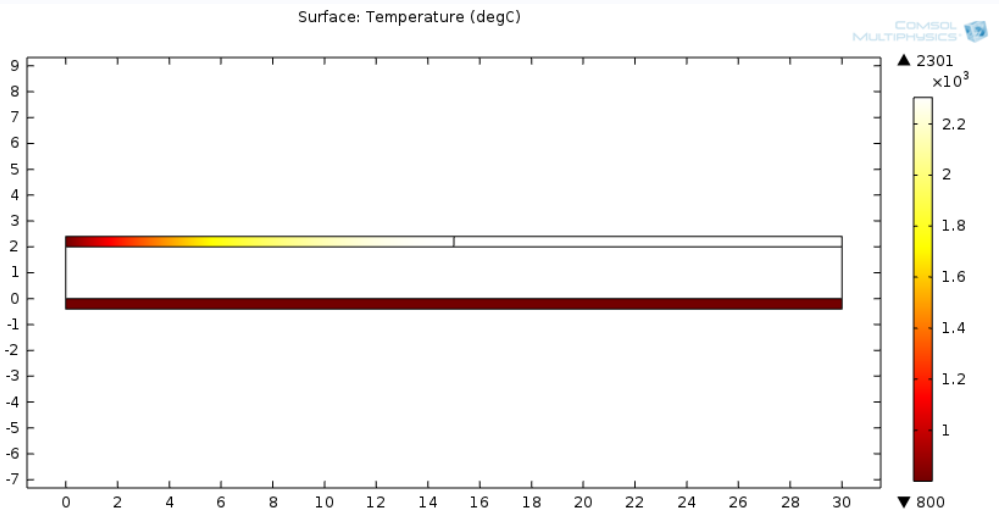

Figure 42 – Temperature distribution along the solid phase.

Once again, since the heat flux is prescribed only in the upper inner wall of the channel and this time only in it first half, only the upper wall exhibit a temperature variation. The solution for the model with fluid and solid phase is presented below with the respective chart and values of temperature on the fluid channel outlet see Figure 43.

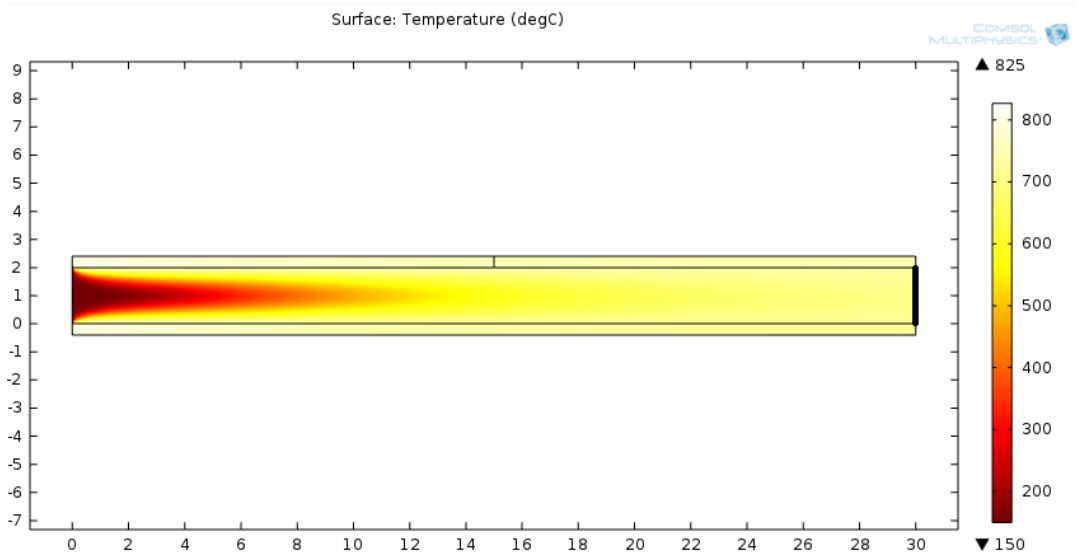

Figure 43 - Temperature profile of the solid and fluid phase.

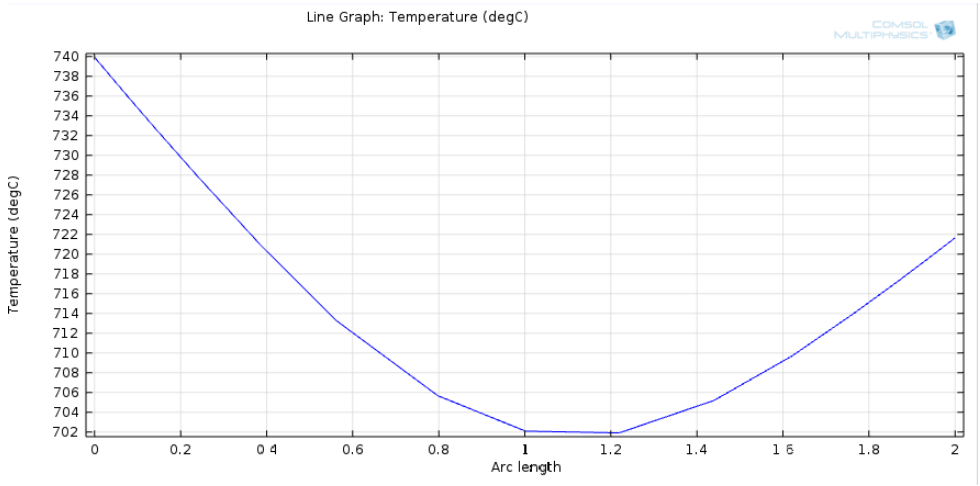

Figure 44– Chart that shows the temperature along the channel outlet.

On the table below, Table 16, it can be observed the temperature of the fluid phase in the outlet of the channel. The values taken from the simulation show a clear difference between considering a heat flux along the length or in an half of the channel. The comparison of the 3 simulations with heat flux in the upper inner wall of the channel will be shown all together in a single table.

Table 16 - Temperature values on the outlet of the channel with respect to the fluid phase.

Average Temperature in the Outlet (˚C)	Maximum Temperature in the Outlet (˚C)	Minimum Temperature in the Outlet (˚C)
713,08	739,94	701,90
Average temperature of the fluid in the channel (˚C)		
605,19		

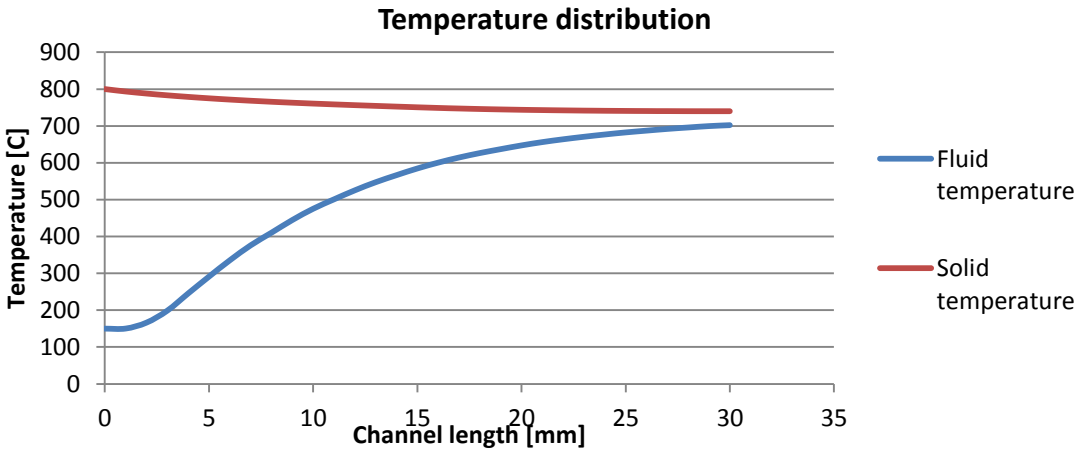

Figure 45 - Fluid and solid temperature distribution along the channel.

6.5.1 Heat flux along one third of the total length of the channel

In this third approach, the most realistic situation is considered, meaning that the concentrated solar radiation has only an effect in a third part of the channel (L/3=10 mm), see Figure 46.

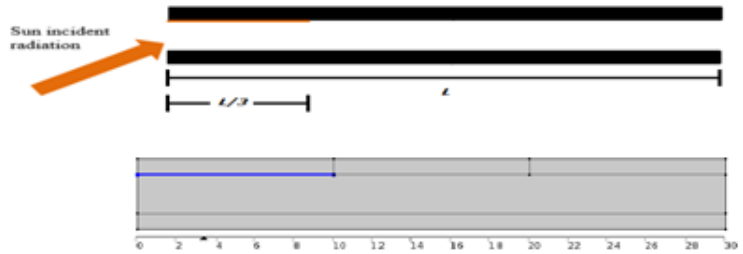

Figure 46 - Heat flux prescribed only in the first third of the channel.

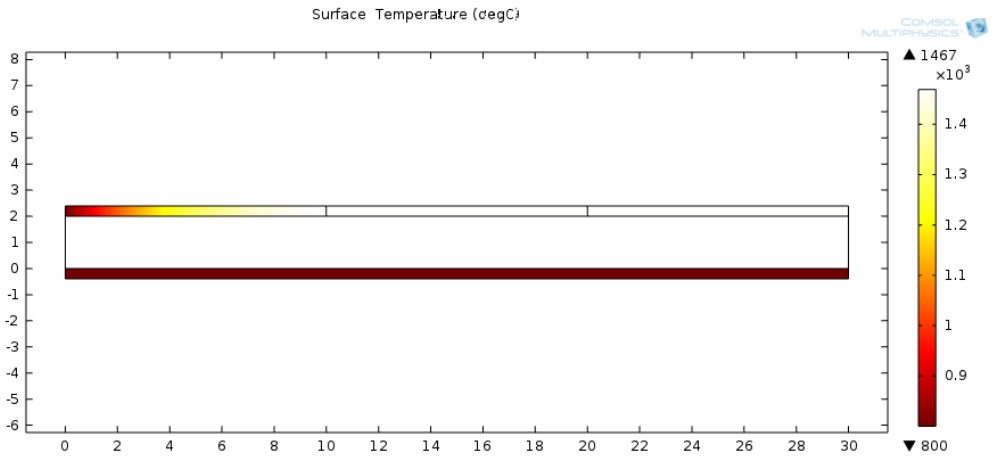

Figure 47 – Solid temperature distribution.

According to the simulations above, only the upper wall exhibit a temperature variation, see Figure 47. The solution shown a solid temperature variation as the other simulation, but the temperature values achieved are lower due the length of the channel where the heat flux is prescribed.

On the fluid and solid phase together solution, the temperature distribution is noticeable as it can be seen in Figure 48 and Figure 49.

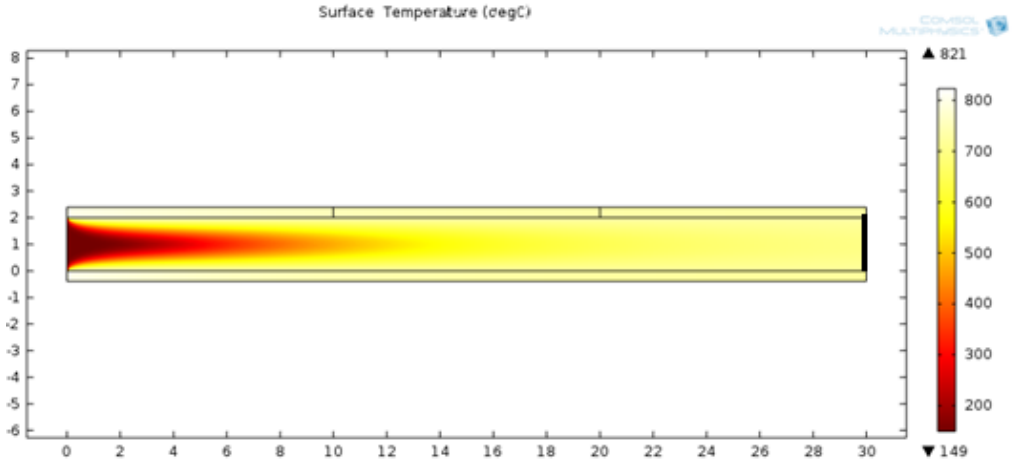

Figure 48 – Temperature distribution of fluid and solid phase.

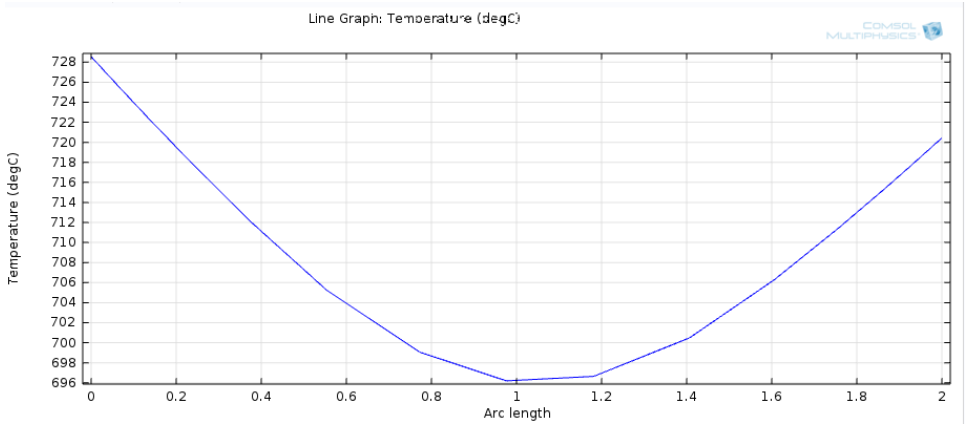

Figure 49 - Chart that shows the temperature along the channel outlet.

The temperature values for the fluid phase were taken in the outlet of the channel and are shown in Table 17 and the respective temperature distribution of both phases is in Figure 50.

Table 17 - Temperature values on the outlet of the channel with respect to the fluid phase.

Average Temperature in the Outlet (˚C)	Maximum Temperature in the Outlet (˚C)	Minimum Temperature in the Outlet (˚C)
706,95	728,55	696,19
Average temperature of the fluid in the channel (˚C)		
601,26		

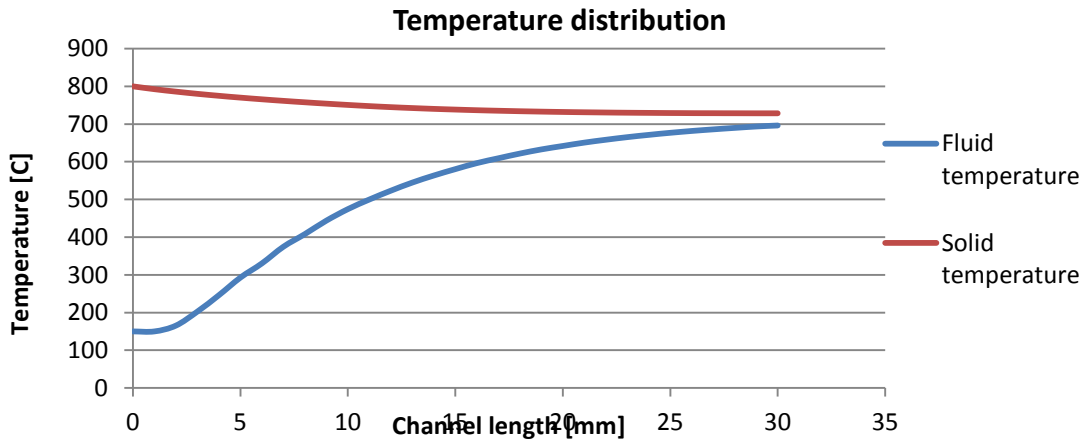

Figure 50 – Temperature distribution of the fluid and solid phase.

As it could be observed in the different temperatures distributions for each phase (solid and fluid) is noticeable that the solid part starts at a higher temperature (at the prescribed temperature) and, along the channel, the temperature decreases. The reverse happens with the fluid phase, in the inlet the temperature is lower and starts increasing along the channel.

Table 18 - Temperature outlet of the 3 simulations with heat flux condition according to the different lengths.

Length	L	L/2	L/3
Temperature	744,02ºC	713,08ºC	706,95ºC

On Table 18, is noticeable the influence of the prescribed heat flux boundary for the fluid temperature. In the most realistic situation which is the situation where the heat flux is prescribed in one third of the total length of the channel, the fluid outlet temperature achieved its about 707ºC. Since the expected values for the solid temperature is around 700ºC, the value achieved in the simulations is a reasonable value.

Since the validation of the model was not possible due the lack of experimental values, these results were compared to the results of a previous study (Smirnova, Fend et al.). The initial conditions of the reference study are shown in Table 19 and the comparison between the temperatures achieved in the model and the reference paper can be observed in Figure 51.

Table 19 - Initial conditions for the simulation in the reference paper.

	Reference paper
T_{fluid}	≈1200 K (≈900ºC)
T_{solid}	≈300 K (≈30ºC)
u_0	≈1 m/s
q_0	1000 MW/m^2

In Figure 51 is represented the physical behaviour of the temperature distribution either for the reference paper either for the simulation (only for one third of the total length of the channel since this was the situation considered as the most realistic situation).

Notice that the values in the figure for the reference paper were taken from the respective paper (Smirnova, Fend et al.) using a tool in order to have a better representation of the comparison between the results on the simulation and in the reference paper. Due this method of obtaining the values of the reference paper, is evident some irregularities in the temperatures distribution. Despite these irregularities, the comparison is perfectly possible.

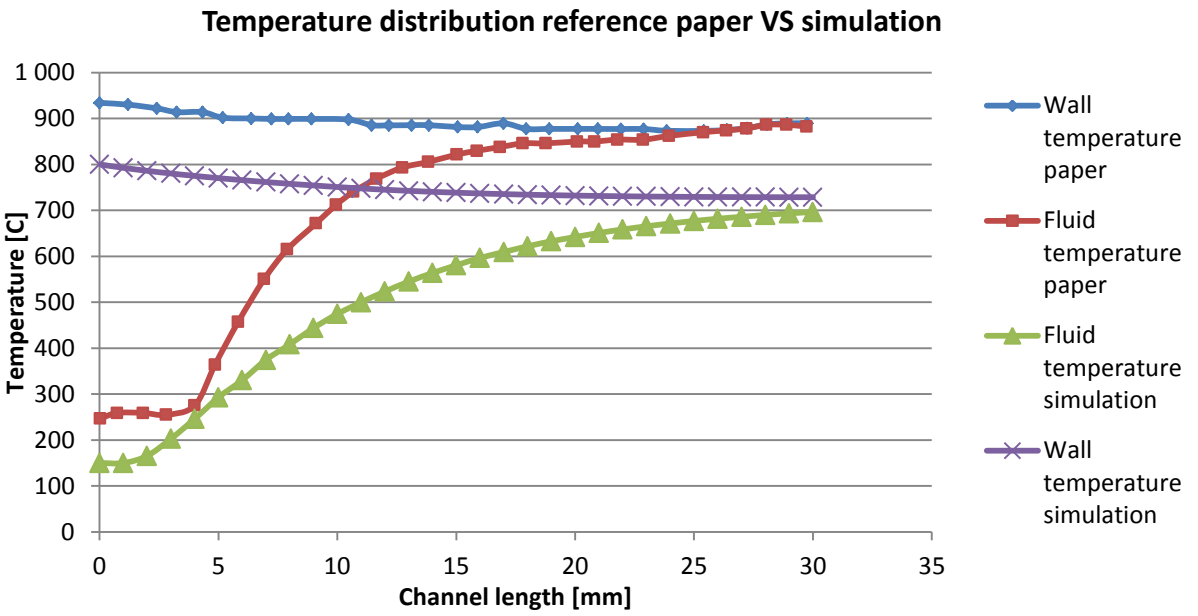

Figure 51 – Chart correspondent to the fluid and solid temperatures of the simulation and the reference paper.

The physical behaviour of the model is identical to the reference paper, i.e., the solid phase decreases the temperature and the fluid phase increases the temperature as it was expected (see again Figure 24).

One of the differences is that in the simulation, the fluid and the solid reach lower temperatures and the solid and the fluid do not attain equal temperatures even though the temperature difference is small. The different temperature distributions along the channel for the fluid and solid between the simulations and in (Olena Smirnova 2010) is a noticeable difference because in the reference paper the temperatures achieved are higher than in the model in discussion. The explanation for this difference, beside the velocity condition and inlet temperature for the fluid and solid is mainly the prescribed flux density which is much bigger for the reference paper (around 1000 MW/m^2) than for the model ($800kW/m^2$).

The effect of the concentrated solar radiation is also noticeable in the different 3 simulations shown before. When the flux is prescribed along the all length of the channel, which is not a representative situation of the reality, the temperatures distributions achieved are much higher than in the other two situations (L/2=15 mm and L/3=10 mm), a difference between each other around 30ºC. Notice that, no heat losses are considered in the model in discussion contrary to what occurs in the reference paper.

The most realistic situation was the one when the heat flux was prescribed only in one third of the total length of the channel (in the inner wall) therefore the model was implemented in a 3D geometry, see Figure 52.

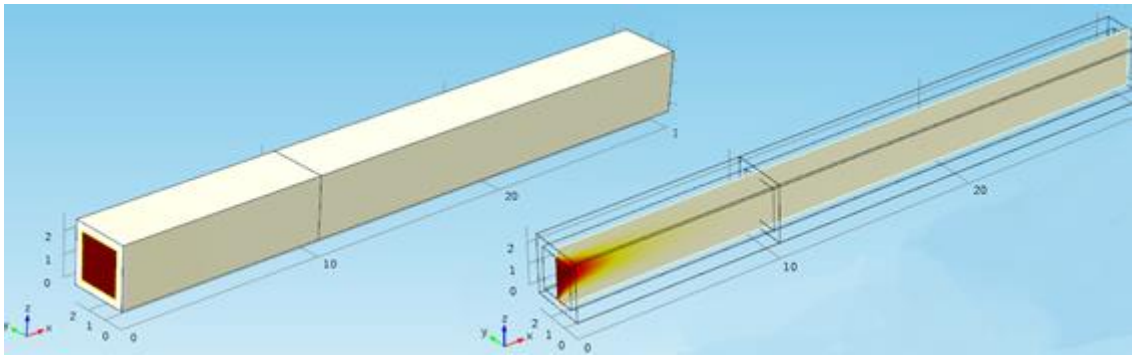

Figure 52 - Temperature distribution in solid and fluid phases in the 3D geometry.

7. Conclusions

The importance of solar energy particularly of solar thermal energy is growing up as well as the technologies around this energy. The main objective of this work, as previously described, was to present a state of the art about the main general technology, Concentrating Solar Power Plants and a description about the air solar receiver technology focusing the main features, parameters and developments and present a model of the conjugate conductive and convective heat transfer in a ceramic receiver honeycomb structure.

This study was carried out considering an input mass flow of 4,18 x 10^{-6} and a 800 kW/m^2 incident heat flux. It was therefore possible to analyse the behaviour of the solid and fluid phases undergoing a conjugate heat transfer. The temperature (°C) distribution has been calculated relatively to the ceramic material and air. Results are shown along the simulation description (chapter 6).

Observing the results shows that higher temperatures are attained in the solid at the inlet of the channel than in the fluid phase because the solid structure is heated up by the incident heat flux at x= 0 mm until x= 10 mm, and heat is then transferred to the remaining solid structure mainly by conduction. The temperature of the fluid flow varies between 150ºC and 745ºC depending on the length where the incident heat flux is considered showing that the heat flux has a strong impact on the temperature distribution. It temperature increases along the length of the channel but solid and fluid never attain equal temperatures contrary to what occurs in the reference paper.

The model implemented shows a good theoretical behaviour and correspondence to the outlet temperature (around 700ºC) although the validation of the model was not possible being this one of the main disadvantage of the model as well as the fact that the thermal losses on the system were neglected (being also a subject for future improvements). The criteria for the mesh used was the time consume and accuracy of the simulations results. Having into account these two parameters, the normal mesh was used.

The study conducted is helpful to study the flow and heat transfer in a honeycomb structure for the volumetric solar air receiver and predict eventual disturbs on the system. The conclusions were drawn from steady state simulations and the validation of the model was not possible with experimental values but was made comparing previous literature.

8. References

Abdelrahman, M., P. Fumeaux and P. Suter (1979). "Study of solid-gas-suspensions used for direct absorption of concentrated solar radiation." Solar Energy **22**(1): 45-48.

Agency, I. E. (2010). "Technology Roadmap Concentrating Solar Power."

Agency, I. E. (2010). Technology Roadmap, Concentrating Solar Power, IEA.

Agrafiotis, C. C., I. Mavroidis, A. G. Konstandopoulos, B. Hoffschmidt, P. Stobbe, M. Romero and V. Fernandez-Quero (2007). "Evaluation of porous silicon carbide monolithic honeycombs as volumetric receivers/collectors of concentrated solar radiation." Solar energy materials and solar cells **91**(6): 474-488.

Ahlbrink, N., J. Andersson, M. Diehl and R. Pitz-Paal (2013). "Optimization of the Mass Flow Rate Distribution of an Open Volumetric Air Receiver." Journal of Solar Energy Engineering **135**(4): 041003.

Aichmayer, L. (2011). "Solar receiver design and verification for small scale polygeneration unit."

Ávila-Marín, A. L. (2011). "Volumetric receivers in solar thermal power plants with central receiver system technology: a review." Solar Energy **85**(5): 891-910.

Becker, M., T. Fend, B. Hoffschmidt, R. Pitz-Paal, O. Reutter, V. Stamatov, M. Steven and D. Trimis (2006). "Theoretical and numerical investigation of flow stability in porous materials applied as volumetric solar receivers." Solar energy **80**(10): 1241-1248.

Burgaleta, J. I., S. Arias and D. Ramirez "GEMASOLAR, THE FIRST TOWER THERMOSOLAR COMMERCIAL PLANT WITH MOLTEN SALT STORAGE."

Center, G. A. (2008). The Jülich Solar Power Tower.

Coggin, S. P. J. D. P. (2013). "Fulfilling the Promise of Concentrating Solar Power." Center for American Progress.

COMSOL. "http://www.comsol.com/video/what-is-comsol-multiphysics."

Council, E. A. S. A. (2011). Concentrating solar power: its potential contribution to a sustainable energy future. www.easac.eu.

DEWITT, D. P. and F. P. INCROPERA (2003). "Fundamentos de Transferência de Calor e de Massa." 5a edição, Ed. LTC, S. Paulo, Brasil.

Fabrizi, F. (2012). "CSP TECHNOLOGIES - ENVIRONMENTAL IMPACT." ENEA - RENEWABLE ENERGY TRAINING PROGRAM.

Fend, T. (2010). "High porosity materials as volumetric receivers for solar energetics."

Fend, T., B. Hoffschmidt, R. Pitz-Paal, O. Reutter and P. Rietbrock (2004). "Porous materials as open volumetric solar receivers: experimental determination of thermophysical and heat transfer properties." Energy **29**(5): 823-833.

Fernandez, V., A. Konstandopoulos, I. Mavroidis, M. Romero, P. Stobbe and F. Téllez "Development of Ceramic Volumetric Receiver Technology."

Flamant, G., D. Gauthier, H. Benoit, J.-L. Sans, B. Boissière, R. Ansart and M. Hemati (2014). "A new heat transfer fluid for concentrating solar systems: Particle flow in tubes." Energy Procedia **49**: 617-626.

Gonzalez-Aguilar, R. O. (2007). ABENGOA, NREL CSP Technology Workshop, Solucar R&D.

Gunther, E. "GUNTHER Portfolio — Photovoltaics, Solar Energy, and Energy Policy." Retrieved 6/11/14, 2014.

Harris, J. A. and T. G. Lenz (1985). "Thermal performance of solar concentrator/cavity receiver systems." Solar Energy **34**(2): 135-142.

Hennecke, K., P. Schwarzbözl, G. Koll, M. Beuter, B. Hoffschmidt, J. Göttsche and T. Hartz (2009). The Solar Power Tower Jülich — A Solar Thermal Power Plant for Test and Demonstration of Air Receiver Technology. Proceedings of ISES World Congress 2007 (Vol. I – Vol. V). D. Y. Goswami and Y. Zhao, Springer Berlin Heidelberg**:** 1749-1753.

Hirsch, T., N. Ahlbrink, J. Gall, V. Nolte, C. Teixeira-Boura and J. Andersson (2012). vICERP: Virtual Institute of Central Receiver Power Plants

Ho, C. K. and B. D. Iverson (2014). "Review of high-temperature central receiver designs for concentrating solar power." Renewable and Sustainable Energy Reviews **29**(0): 835-846.

Ho, C. K. and B. D. Iverson (2014). "Review of high-temperature central receiver designs for concentrating solar power." Renewable and Sustainable Energy Reviews **29**: 835-846.

Hoffschmidt, B., R. Pitz-Paal, M. Bohmer, T. Fend and P. Rietbrock (1999). 200 KWTH OPEN VOLUMETRIC AIR RECEIVER (HITREC) OF DLR REACHED 1000 C AVERAGE OUTLET TEMPERATURE AT PSA. Les Ulis, FRANCE, EDP sciences.
Hoffschmidt, B., F. l. M. Téllez, A. Valverde, J. s. Fernández and V. Fernández (2003). "Performance evaluation of the 200-kWth HiTRec-II open volumetric air receiver." Journal of solar energy engineering **125**(1): 87-94.
Hunt, A. J. (2012). Development of a New High Temperature Gas Receiver Utilizing Small Particles. International Symposium on Solar Thermal Power and Energy Systems, Marseille, France, June 15-20, 1980.
Karni, J., A. Kribus, P. Doron, R. Rubin, A. Fiterman and D. Sagie (1997). "The DIAPR: a high-pressure, high-temperature solar receiver." Journal of solar energy engineering **119**(1): 74-78.
Lovegrove, K. and W. Stein (2012). Concentrating Solar Power Technology: Principes, developments and applications, Elsevier.
Lovegrove, K. and W. Stein (2012). Concentrating solar power technology: principles, developments and applications, Elsevier.
Menigault, T., G. Flamant and B. Rivoire (1991). "Advanced high-temperature two-slab selective volumetric receiver." Solar energy materials **24**(1): 192-203.
Miller, F. and R. Koenigsdorff (1991). "Theoretical analysis of a high-temperature small-particle solar receiver." Solar energy materials **24**(1): 210-221.
Miller, F. J. and A. J. Hunt (2012). Developing the Small Particle Heat Exchange Receiver for a Prototype Test. ASME 2012 6th International Conference on Energy Sustainability collocated with the ASME 2012 10th International Conference on Fuel Cell Science, Engineering and Technology, American Society of Mechanical Engineers.
Miller, F. J. and R. W. Koenigsdorff (2000). "Thermal modeling of a small-particle solar central receiver." Journal of solar energy engineering **122**(1): 23-29.
Multiphysics, C. (2013). Introduction to COMSOL Multiphysics.
Olena Smirnova, T. F., Schwarzbözl Peter, Daniel Schöllgen (2010). Homogeneous and Inhomogeneous Model for Flow and Heat Transfer in Porous Materials as High Temperature Solar Air Receivers. COMSOL Conference. Paris.
Olena Smirnova, T. F., Schwarzbözl Peter, Daniel Schöllgen (2010). Homogeneous and Inhomogeneous Model for Flow and Heat Transfer in Porous Materials as High Temperature Solar Air Receivers. Proceedings of the COMSOL Conference Paris 2010. C. Multiphysics. Paris.
Palero, S., M. Romero and J. L. Castillo (2008). "Comparison of experimental and numerical air temperature distributions behind a cylindrical volumetric solar absorber module." Journal of Solar Energy Engineering **130**(1): 011011.
Research, G. A. C. D. I. o. S. (2013). Solar thermal power plants, utilising concentrated sunlight for generating energy.
Romero, M., R. Buck and J. E. Pacheco (2002). "An update on solar central receiver systems, projects, and technologies." Journal of Solar Energy Engineering **124**(2): 98-108.
Sano, Y. and S. Iwase "Optimal Design of a Silicon Carbide Ceramic Foam Solar Volumetric Receiver."
Scheffler, M. and P. Colombo (2006). Cellular ceramics: structure, manufacturing, properties and applications, John Wiley & Sons.
Siegel, R. and J. Howell (2002). Thermal Radiation Heat Transfer, Taylor&Francis.
Singh, H., R. Saini and J. Saini (2010). "A review on packed bed solar energy storage systems." Renewable and Sustainable Energy Reviews **14**(3): 1059-1069.
Smirnova, O., T. Fend, S. Peter and D. Schöllgen Homogeneous and inhomogeneous model for flow and heat transfer in porous materials as high temperature solar air receivers.
SOLAR, A. (2010). Solar Power for a Sustainable World, CIT Andalucía VII FP-Energy: Solugas.
Spelling, J., D. Favrat, A. Martin and G. Augsburger (2012). "Thermoeconomic optimization of a combined-cycle solar tower power plant." Energy **41**(1): 113-120.
Vogel, W. and H. Kalb (2010). Large-scale solar thermal power: technologies, costs and development, John Wiley & Sons.

Wang, F., Y. Shuai, H. Tan and C. Yu (2013). "Thermal performance analysis of porous media receiver with concentrated solar irradiation." International Journal of Heat and Mass Transfer **62**: 247-254.
Winter, C. J., R. L. Sizmann and L. L. Vant-Hull (1991). Solar Power Plants, Springer Berlin Heidelberg.
Wu, Z., C. Caliot, G. Flamant and Z. Wang (2011). "Coupled radiation and flow modeling in ceramic foam volumetric solar air receivers." Solar Energy **85**(9): 2374-2385.
Xu, H. (2013). "Numerical Study on the Thermal Performance of a Novel Impinging Type Solar Receiver for Solar Dish-Brayton System."